AWARD NUMBER: W81XWH-19-1-0123

TITLE: **Stalled Replication Fork Protection Defects as a Predictor of Therapeutic Response**

PRINCIPAL INVESTIGATOR: Sarah Hill

CONTRACTING ORGANIZATION: Dana-Farber Cancer Institute, Inc.
450 Brookline Avenue, Boston, MA 02115-5418

REPORT DATE: MAY 2021

TYPE OF REPORT: Annual Report

PREPARED FOR: U.S. Army Medical Research ACQ Activity
820 Chandler Street, Fort Detrick, MD 21702-5012

DISTRIBUTION STATEMENT: Approved for Public Release;
Distribution Unlimited

The views, opinions and/or findings contained in this report are those of the author(s) and should not be construed as an official Department of the Army position, policy or decision unless so designated by other documentation.

REPORT DOCUMENTATION PAGE

Form Approved
OMB No. 0704-0188

1. REPORT DATE	2. REPORT TYPE	3. DATES COVERED
MAY 2021	Annual	5/1/20– 4/30/21

4. TITLE AND SUBTITLE

Stalled Replication Fork Protection Defects as a Predictor of Therapeutic Response

5a. CONTRACT NUMBER
W81XWH-19-1-0123

5b. GRANT NUMBER
W81XWH-19-1-0123

5c. PROGRAM ELEMENT NUMBER

6. AUTHOR(S)
Sarah Hill

E-Mail: Sarah_hill@dfci.harvard.edu

5d. PROJECT NUMBER
0011294269

5e. TASK NUMBER

5f. WORK UNIT NUMBER

7. PERFORMING ORGANIZATION NAME(S) AND ADDRESS(ES)
Dana-Farber Cancer Institute, Inc.
450 Brookline Avenue
Boston, MA 02215-5418

8. PERFORMING ORGANIZATION REPORT NUMBER

9. SPONSORING / MONITORING AGENCY NAME(S) AND ADDRESS(ES)

U.S. Army Medical Research and Development
Command Fort Detrick, Maryland 21702-5012

10. SPONSOR/MONITOR'S ACRONYM(S)

11. SPONSOR/MONITOR'S REPORT NUMBER(S)

12. DISTRIBUTION / AVAILABILITY STATEMENT

Approved for Public Release; Distribution Unlimited

13. SUPPLEMENTARY NOTES

14. ABSTRACT: The major goals of this award are to study prevalence and mechanisms of stalled replication fork protection defects in high grade serous ovarian cancer (HGSC) using patient derived organoid models. The goals of the three Aims included generating and characterizing the organoids, profiling the DNA damage repair capacity of the organoids, and determining if there is synergy between DNA damage repair defect therapies and immune therapies. Progress has been made in all aims this year despite the COVID pandemic. Thus far we have generated twenty HGSC organoid cultures and validated them as being matches to their parent tumors. We also profiled the DNA damage repair capacity of these cultures and demonstrated that the majority were proficient in homologous recombination and some deficient in stalled replication fork protection and that these fork protection defects correlated with sensitivity to specific DNA damage repair therapies. We are following all patients from whom organoids are generated and comparing the organoid outcomes with the patient outcomes. In addition, we have tested for activation of the replication stress response in various tumors after single or combination DNA damage repair therapies. We have not identified a common mechanism within ATR signaling which is an overarching signaling pathway in replication stress. We have identified the bromodomain containing protein BRD1 as possibly being important in the replication stress response in HGSC. We continue to work up the mechanism of action of BRD1 and other hits from our RNA sequencing in the HGSC replication stress response. Finally, we immune profiled multiple parent tumors and matched organoid/immune cell co-cultures by flow cytometry and one also by single cell RNA sequencing and demonstrated that the organoid co-cultures are accurate models of the parent tumors. We performed flow cytometry and ELISA functional analyses on these co-cultures and found that immunotherapies do induce an immune response in these cultures and were able to determine that BRD1 depletion by some of these immune therapies is the mechanism by which these therapies bring intra-tumoral immune cells back from exhaustion. We determined that BRD1 inhibitors may be an effective immune therapy in HGSC either alone or in combinations and published these findings in a recent manuscript (PMID: 33158814).

15. SUBJECT TERMS
HGSC, DNA damage

16. SECURITY CLASSIFICATION OF:			17. LIMITATION OF ABSTRACT	18. NUMBER OF PAGES	19a. NAME OF RESPONSIBLE PERSON USAMRMC
a. REPORT	**b. ABSTRACT**	**c. THIS PAGE**	Unclassified	36	**19b. TELEPHONE NUMBER** *(include area code)*
Unclassified	Unclassified	Unclassified			

Standard Form 298 (Rev. 8-98)
Prescribed by ANSI Std. Z39.18

TABLE OF CONTENTS

1. **INTRODUCTION:** *Narrative that briefly (one paragraph) describes the subject, purpose and scope of the research.*

Fifty percent of high grade serous ovarian cancers (HGSC) carry a genomic alteration in a DNA damage repair gene. Through recent functional analysis on a limited number of patient derived HGSC organoids, my lab has demonstrated that the majority of these mutations confer defects in protection/repair of stalled replication forks and not in repair of double strand breaks by homologous recombination as previously thought. Based on this preliminary work we hypothesized that stalled replication fork protection defects are more prevalent than HR defects in HGSC and that therapies targeting such a defect may offer benefit to a larger patient population. The major goal of this work is to use HGSC organoids to understand the importance of fork instability in HGSC, uncover mechanisms leading to fork instability, and determine how such functional defects lead to different types of therapeutic sensitivities, including immune therapies.

2. **KEYWORDS:** *Provide a brief list of keywords (limit to 20 words).*

High grade serous ovarian cancer, DNA damage, stalled replication forks, double strand breaks, homologous recombination, BRCA1, BRCA2, immune therapy, PD-1

3. **ACCOMPLISHMENTS:** *The PI is reminded that the recipient organization is required to obtain prior written approval from the awarding agency grants official whenever there are significant changes in the project or its direction.*

What were the major goals of the project?
List the major goals of the project as stated in the approved SOW. If the application listed milestones/target dates for important activities or phases of the project, identify these dates and show actual completion dates or the percentage of completion.

-Please note that this award was not started until 11/6/19 due to HRPO approval delays until that date. We experienced significant delays due to a COVID shutdown of Dana-Farber between March and June of 2020 and continued delays in obtaining human tissue for organoid generation continuing through September 2020. Tissue acquisition normalized in the Fall of 2020, and we were able to resume organoid generation successfully at that time. We have requested a one year NCE to complete the work in our SOW.
Major Task 1: Generation of 100 patient derived human organoid lines from patients on relevant treatments: This task is 20% complete.
Major Task 2: Repair defect characterization of organoids: This task is 20% complete.
Major Task 3: Assess methods of fork destabilization in both fork stable and unstable organoid cultures: This task is 20% complete.
Major Task 4: Assess what other pathways might lead to fork instability in different repair defect backgrounds: This task is 50% complete.
Major Task 5: Immune phenotype parent tumors and organoid cultures in various settings: This task is 50% complete and a publication has been generated (see attached).
Major Task 6: Cytokine profile parent tumors and organoid cultures in various settings This task is 50% complete and a publication has been generated (see attached).

What was accomplished under these goals?

For this reporting period describe: 1) major activities; 2) specific objectives; 3) significant results or key outcomes, including major findings, developments, or conclusions (both positive and negative); and/or 4) other achievements. Include a discussion of stated goals not met. Description shall include pertinent data and graphs in sufficient detail to explain any significant results achieved. A succinct description of the methodology used shall be provided. As the project progresses to completion, the emphasis in reporting in this section should shift from reporting activities to reporting accomplishments.

-Please note that this award was not started until 11/6/19 due to HRPO approval delays until that date. We experienced significant delays due to a COVID shutdown of Dana-Farber between March and June of 2020 and continued delays in obtaining human tissue for organoid generation continuing through September 2020. Tissue acquisition normalized in the Fall of 2020, and we were able to resume organoid generation successfully at that time. We have requested a one year NCE to complete the work in our SOW.

Major Task 1: Generation of 100 patient derived human organoid lines from patients on relevant treatments:

1) The major activities that occurred in this task were the generation and characterization of HGSC organoids.

2) Our objective is to generate and profile enough organoids to determine prevalence of stalled replication fork protection defects, correlations with therapeutic response in patients, and correlations with specific therapies or genomic alterations.

3) We were able to generate and histologically profile 8 new HGSC organoid lines since tissue collection resumed in Fall 2020, brining our total to 20. We have now started working with the Center for Patient Derived Models at Dana-Farber Cancer Institute to genomically profile the organoids. For each organoid and parent tumor, we are currently performing STR profiling to ensure that they both match each other and are not contaminated with other lines. We are also performing low pass whole genome sequencing to examine copy number alterations and targeted panel whole exome sequencing to search for key somatic alterations (e.g. *BRCA1*). So far, four of our organoid lines have completed this sequencing, and we will continue genomically profiling all lines generated in the coming year. Working with this DFCI internal core facility became our best option due to COVID restrictions, and thus far we have had success in determining that one of our lines carries a *BRCA1* alteration. We will continue to generate organoids with all available tissue this coming year. All organoids generated thus far demonstrated p53 mutations, PAX8 positivity, and morphologic characteristics similar to the parent tumors.

4) An additional achievement in this task, is that we have begun a collaboration with Anthony Letai's lab at Dana-Farber in which we are also using BH3 profiling to study the response of organoids generated in Task 1 to drugs. Normally, we use Cell Titer Glo to measure ATP in the cells after dose curve drug treatments to establish sensitivity, and these were the sensitivities we had been using to match to patients. The Letai lab studies apoptosis and uses BH3 profiling to measure the apoptotic response of tumor cells to drugs. With Dr. Letai, we have now, in addition to our own Cell Titer Glo profiling, performed BH3 profiling on 10 of our lines. We are excited to report that the BH3 profiling appears to more accurately reflect patient response than the Cell Titer Glo measurements. We will continue to provide organoids to the Letai lab and plan to submit a manuscript detailing the comparison our Cell Titer Glo to his BH3 profiling of the organoids in response to Carboplatin and how this matches patient response later this year.

Overall, the work in this task is moving forward and provided us with organoid lines to work with in all other Aims.

Major Task 2: Repair defect characterization of organoids:
1) The major activities in this task are to profile the stalled fork protection capacity, homologous recombination capacity, DNA damage genomic traits, and sensitivity to DNA damage therapies of the organoid lines generated in task 1.
2) The objective is to utilize these findings to compare to patient outcomes which will help determine which, if any, organoid assays may mimic patient response.
3) The major results in this task are that we have profiled the repair capacity of our 20 organoid cultures by performing replication combing assays, RAD51 focus formation assays, and testing the cultures for sensitivity to carboplatin, gemcitabine, and a PARP and ATR inhibitor. Out of the 20 lines none appears to be HR defective, but more than half have stalled fork protection defects by the fiber assays and are more sensitive to replication stress inducing agents such as gemcitabine.
4) We continue the work in this aim with every new line generated.

Major Task 3: Assess methods of fork destabilization in both fork stable and unstable organoid cultures:
1) The major activities in this task are to use western blots and replication combing assays to study replication stress in our organoid cultures in the setting of drug combination treatment with the hope that perhaps specific combinations can destabilize replication forks and cause cytotoxicity even in fork stable lines.
2) The objective of this task is to determine if combination therapies may be utilized even in therapy resistant patients by defining combinations which can induce DNA damage repair defects.
3) The major results in this task so far are that in the 20 cultures, it is apparent that classic replication stress markers like phosphorylated RPA or phosphorylated KAP1 are upregulated at different times post-treatment with single or combination replication stress inducing agents. It is not clear yet if the speed of upregulation is dictating therapeutic response.

Major Task 4: Assess what other pathways might lead to fork instability in different repair defect backgrounds
1) The major activities in this task were to explore mechanisms of fork protection defects in different organoid lines through bulk RNA sequencing of select lines after treatment with replication stress inducing agents. The mechanisms are then tested and validated in the organoids.
2) The goal of this task is to understand mechanisms of replication fork protection defects in HGSC, and in so doing, potentially generate better therapies to target the specific defects.
3) In our recent publication, Wan and Hill, *Cancer Research* 2020 PMID: 33158814, we identified a protein called BRD1 as being an important target for immune therapies in HGSC. However, in addition to studying the role of BRD1 in immune cells, we also began to examine its function in HGSC tumor cells. BRD1 is a bromodomain containing protein known to function in epigenetic regulation of many different genes in different cell types. Nothing is known about its role in HGSC tumor cells. As part of a control for our work studying BRD1 inhibition in immune cells, we tested for sensitivity to the BRD1 inhibitor BAY 299 in a small set of HGSC organoids and cell lines compared to T and NK cell lines (Figure 1)
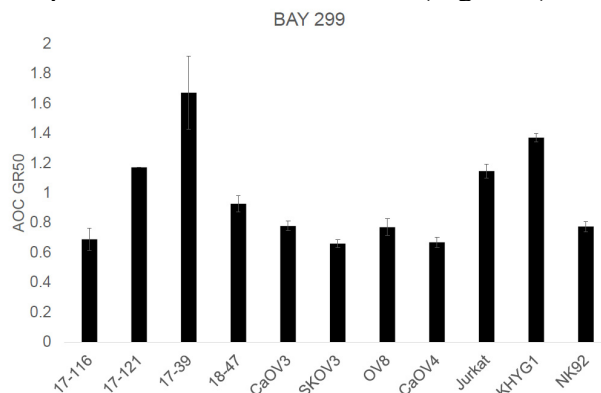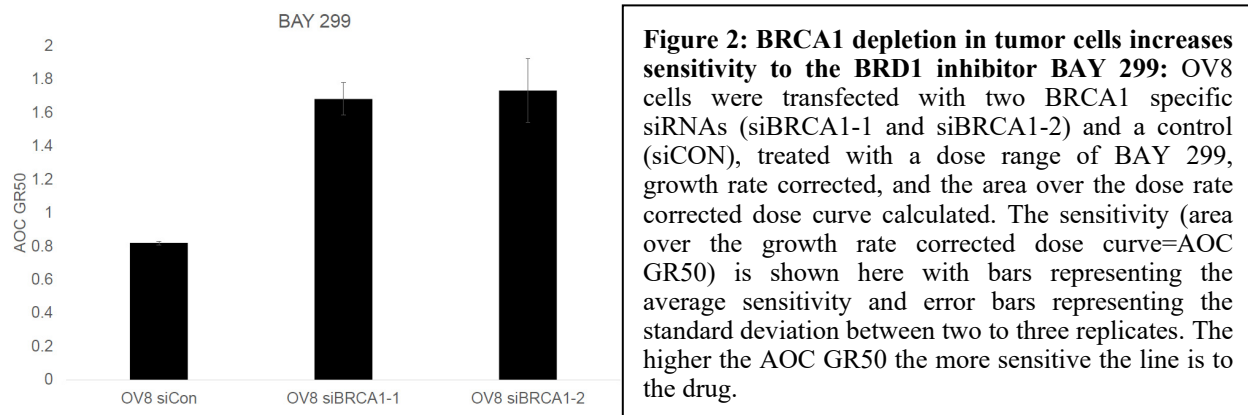

Figure 1: BRCA1 deficiency in tumor cells increases sensitivity to the BRD1 inhibitor BAY 299: A panel of HGSC organoids (17-116, 17-121, 17-39, and 18-47) and cell lines (CaOV3, SKOV3, OV8, CaOV4) compared to T (Jurkat) and NK (KHYG1 and NK92) cell lines were tested for sensitivity to the BRD1 inhibitor BAY 299. All lines were growth rate corrected to allow for easy comparison. The sensitivity (area over the growth rate corrected dose curve=AOC GR50) is shown here with bars representing the average sensitivity and error bars representing the standard deviation between two to three replicates. The higher the AOC GR50 the more sensitive the line is to the drug.

We were surprised to find that our *BRCA1* mutant organoid line 17-39 showed the greatest sensitivity to BRD1 inhibition compared to all other cells suggesting possible synthetic lethality between BRD1 inhibition and *BRCA1* functional loss. To validate this possibility we transfected a standard *BRCA1* wildtype HGSC cell line with two different *BRCA1* specific siRNAs and tested the cells for sensitivity to BAY 299 compared to a control transfected line Figure 2.

Figure 2: BRCA1 depletion in tumor cells increases sensitivity to the BRD1 inhibitor BAY 299: OV8 cells were transfected with two BRCA1 specific siRNAs (siBRCA1-1 and siBRCA1-2) and a control (siCON), treated with a dose range of BAY 299, growth rate corrected, and the area over the dose rate corrected dose curve calculated. The sensitivity (area over the growth rate corrected dose curve=AOC GR50) is shown here with bars representing the average sensitivity and error bars representing the standard deviation between two to three replicates. The higher the AOC GR50 the more sensitive the line is to the drug.

Based on these findings, we hypothesize that BRD1 inhibition may be leading to chromatin changes that increase DNA damage possibly by altering stalled replication fork protection. In addition to our previously reported hits, in this NCE year we will also explore the role of BRD1 at stalled replication forks or in fork protection given its connection to our recent publication. This may provide a more indirect role for a protein in fork protection in controlling chromatin state rather than being part of the actual fork protection machinery.

Major Task 5: Immune phenotype parent tumors and organoid cultures in various settings:
1) The major activities in this task were to immune profile parent tumors and treated organoid cultures and have been detailed in our recent publication (PMID: 33158814).
2) The objectives were to be certain that the organoids matched the parent tumors and also to determine if organoid cultures treated with immune therapies alone or in combination with DNA damage repair therapies showed increased tumor cell death with any single agents or combinations.
3) Parent tumors and untreated organoid/immune cell co-cultures were compared to each other by both flow cytometry and single cell RNA sequencing (Figure 3).
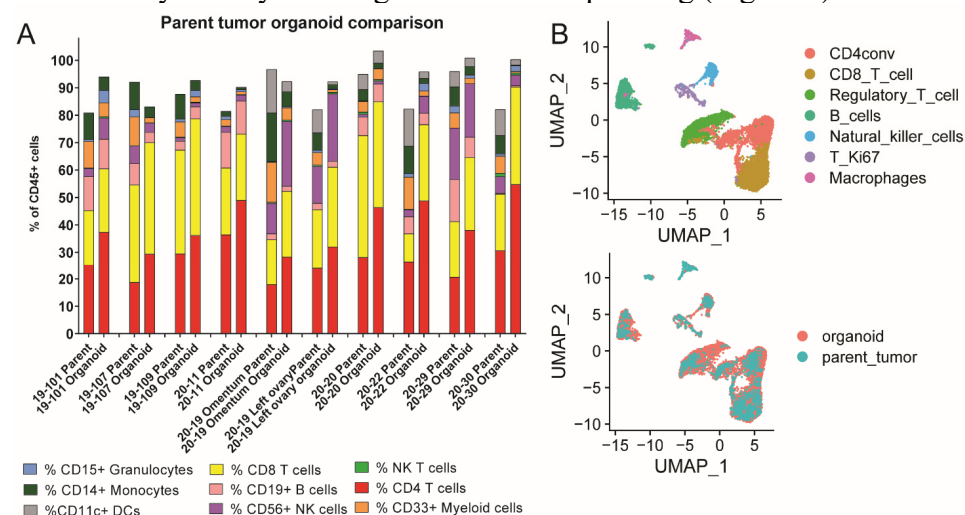

FIGURE 3: Organoid co-cultures resemble parent tumor immune composition: A) Ten short term organoid co-cultures were established, and flow cytometry analysis for all immune lineages of the parent tumor compared to the organoid co-culture was performed at 96 hours post-plating. Flow for dendritic cells was not performed for the first four tumors in the graph. The parent tumor and organoid composition are shown side by side here for each tumor as a percentage of CD45+ cells. **B)** Single cell RNA sequencing analysis was performed on all viable CD45 positive cells from a single parent tumor and organoid co-culture. The top panel shows all cells detected across both samples, and the bottom panel shows an overlay of all cells detected in the parent tumor and organoid co-culture. CD4conv=Conventional non-regulatory CD4 T cells, T_Ki67=proliferating CD8 T cells, Regulatory_T_cell=CD4 Regulatory T cells

We generate these cultures after gentle mechanical disruption of tumors obtained directly from the operating room and then utilize the cultures for various immune functional assays to study anti-tumor immune activity in response to various targeted therapies (PMID: 33158814). In our initial work, we found that the organoid co-cultures contained all of the immune cell types present in the parent tumors at similar ratios by both flow cytometry and single cell RNA sequencing making them faithful models of their parent tumors (Figure 3). In our recent publication we then utilized the co-cultures to study the effects of a novel bispecific anti-PD-1/PD-L1 antibody on all immune cells in the culture in comparison to the single arm anti-PD-1 or anti-PD-L1 controls or an isotype control. There were no obvious changes in cell types or cell numbers in these settings, but we did find increased activity in specific subsets of CD8 T cells and in NK cells in response to the bispecific antibody (PMID: 33158814), and this was a result of decreased expression of the bromodomain containing protein BRD1 induced by the bispecific antibody (PMID: 33158814).

We are now starting to perform flow cytometry profiling on the organoid co-cultures after treatment with the common anti-PD-1 antibody Pembrolizumab or with our BRD1 inhibitor BAY 299 in combination with DNA damage repair agents like carboplatin or gemcitabine.

4) The results from this initial work resulted in the first publication from the Hill lab (PMID: 33158814), and this paper won an award at the recent AACR Annual meeting, the *Cancer Research* Early Career Award (https://cancerres.aacrjournals.org/award).

Major Task 6: Cytokine profile parent tumors and organoid cultures in various settings
1) The major activities in this task were to perform cytokine profiling of the parent tumors and organoids.
2) The objective was to demonstrate that the parent tumors and organoids match and that the organoids demonstrate cytokine alterations post treatment with ICB agents alone or in combination with DNA damage repair agents.
3) We started assessing organoid response to ICB agents including a novel bispecific anti-PD-1/PD-L1 antibody on all immune cells in the culture in comparison to the single arm anti-PD-1 or anti-PD-L1 controls or an isotype control using interferon gamma (IFNγ) ELISA after a standard timepoint (Figure 4)
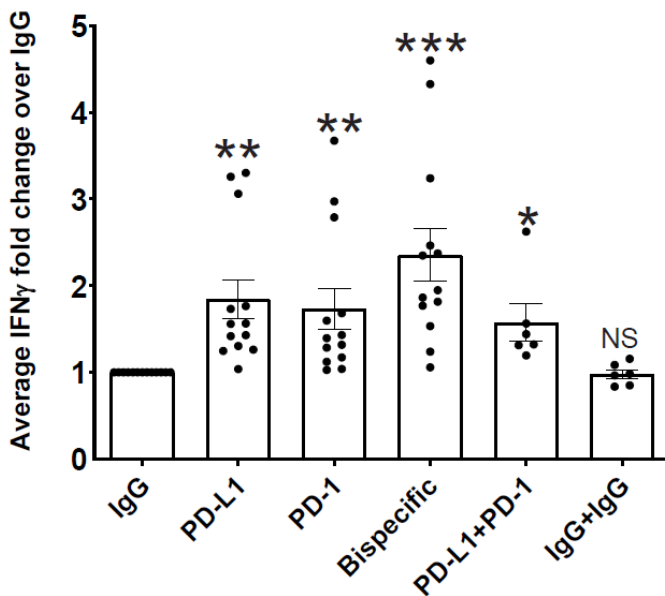

Figure 4: Organoid co-cultures demonstrate an immune response when treated with ICB agents: The organoid cultures profiled in Figure 3 were treated with either an IgG control, anti-PD-L1, anti-PD-1, a bispecific anti-PD-1/PD-L1 antibody, anti-PD-1+anti-PD-L1 or IgG+IgG. Media was harvested after a standard amount of time for each culture, and the media was subject to IFNγ ELISA. Average IFNγ amounts normalized to the IgG control are shown here across all experiments with error bars representing standard error of the mean. p-values were calculated for all comparisons using a paired t-test. Comparisons of key antibodies to the IgG control are shown. *<0.05, **<0.005, ***<0.0005.

Single cell RNA sequencing analysis later revealed that this increased IFNγ production induced by the bispecific antibody was due to downregulation of BRD1 (PMID: 33158814). Thus we tested a BRD1 inhibitor or vehicle in combination with these four antibodies and found that the BRD1 inhibitor increased IFNγ production when combined with isotype control, anti-PD-L1, or anti-PD-1 (Figure 5) suggesting that the BRD1 inhibitor either alone or in combination with ICB agents might be a useful immune therapy in HGSC.
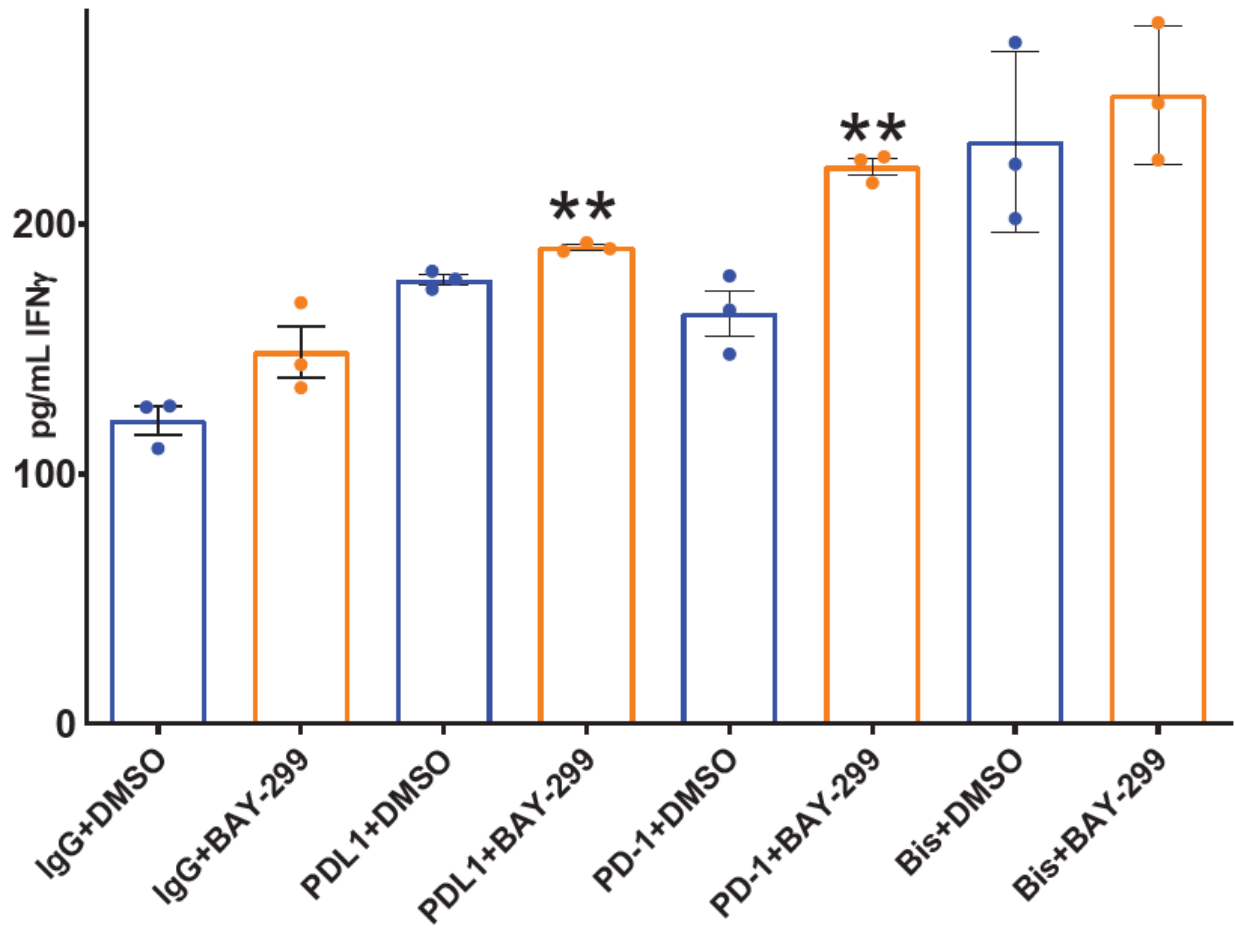

Figure 5 BRD1 inhibition causes increased immune activity at baseline or in combination with specific immune checkpoint blockade agents: An organoid co-culture was treated with isotype control, anti-PD-1, anti-PD-L1, or anti-PD-1/PD-L1 combined with either DMSO (blue) or the BRD1 inhibitor BAY-299 (orange). The co-culture media supernatants underwent IFNγ ELISA analysis shown here as the average pg/mL of IFNγ for the treatment with error bars representing standard error. **p<0.005

We were able to show by flow cytometry that the BRD1 inhibitor caused decreased exhaustion in T and NK cells to cause this increased IFNγ production (PMID: 33158814). To test whether the BRD1 inhibitor was an effective immune therapy *in vivo*, we studied the efficacy of the BRD1 inhibitor in decreasing tumor burden and increasing immune activity in a syngeneic HGSC mouse model (PMID: 33158814). We found that the BRD1 inhibitor did lead to a significantly decreased tumor burden in these animals and that this was due to decreased T and NK cell exhaustion (PMID: 33158814). These findings validated the efficacy of BRD1 inhibition as an immune therapy in HGSC and also highlighted how effective the co-culture system is in studying the anti-tumor response in HGSC.

Knowing that cytokine response to immune stimulation can be effectively detected in these co-cultures and that this stimulation does reflect an *in vivo* response, we now plan to use the co-cultures to test ICB agents or even the BRD1 inhibitor in combination with DNA damage repair defect targeting agents.

We hope to perform these same types of analysis with IFNγ and later multi-plex ELISA analysis on organoid co-cultures treated with Pembrolizumab or BRD1 inhibitor combined with DNA damage repair agents.

4) An additional achievement based on results from this Aim is a published manuscript detailing the work above (PMID: 33158814).

What opportunities for training and professional development has the project provided?

If the project was not intended to provide training and professional development opportunities or there is nothing significant to report during this reporting period, state "Nothing to Report."

Describe opportunities for training and professional development provided to anyone who worked on the project or anyone who was involved in the activities supported by the project. "Training" activities are those in which individuals with advanced professional skills and experience assist others in attaining greater proficiency. Training activities may include, for example, courses or one-on-one work with a mentor. "Professional development" activities result in increased knowledge or skill in one's area of expertise and may include workshops, conferences, seminars, study groups, and individual study. Include participation in conferences, workshops, and seminars not listed under major activities.

Training activities for the PI fostered by this award included the opportunity for Dr. Hill who is a junior faculty member to train her research technician. Being able to train others to perform scientific tasks is critical to success as an independent investigator.

How were the results disseminated to communities of interest?
If there is nothing significant to report during this reporting period, state "Nothing to Report."

Describe how the results were disseminated to communities of interest. Include any outreach activities that were undertaken to reach members of communities who are not usually aware of these project activities, for the purpose of enhancing public understanding and increasing interest in learning and careers in science, technology, and the humanities.

-7-14-20-Dr. Hill presented this work at the Englander Institute for Precision Medicine at Cornell
-10/14/20-Dr. Hill presented this work for the Society for Functional Precision Medicine

What do you plan to do during the next reporting period to accomplish the goals?
If this is the final report, state "Nothing to Report."

Describe briefly what you plan to do during the next reporting period to accomplish the goals and objectives.

For Aim 1 (Task 1), we plan to generate and profile the remaining organoid cultures specified in our proposal.

For Aim 2 (Tasks 2-4), we plan to profile the DNA damage repair capacity of the remaining organoids we generate and compare these results to patient outcomes to both determine prevalence of different types of repair defects and understand if any specific organoid assays may help predict patient response. We will also continue to test DNA damage repair agent combinations in our cultures to help determine if specific combinations will be useful in treating patients who may be resistant to DNA damage repair therapies because the tumor lacks a repair defect. Finally, we plan to study the mechanisms of replication fork protection defects by further studying BRD1 which was discovered as both an immune therapy target and a DNA damage repair protein in our recent publication and also unpublished data.

For Aim 3 (Tasks 5-6) we have our immune profiling system functioning well and have already published a manuscript with our findings during this past funding year. Our goal in the next year is to test more DNA damage repair agent/ICB combinations, including our recently discovered anti-BRD1 small molecule therapy, to determine which combinations are most effective in organoids which have DNA damage repair defects.

4. **IMPACT:** D*escribe distinctive contributions, major accomplishments, innovations, successes, or any change in practice or behavior that has come about as a result of the project relative to:*

What was the impact on the development of the principal discipline(s) of the project?
If there is nothing significant to report during this reporting period, state "Nothing to Report."

Describe how findings, results, techniques that were developed or extended, or other products from the project made an impact or are likely to make an impact on the base of knowledge, theory, and research in the principal disciplinary field(s) of the project. Summarize using language that an intelligent lay audience can understand (Scientific American style).

The major findings from this work so far have to do with high grade serous ovarian cancer response to immune therapies. Our work in Tasks 5 and 6 allowed us to immune profile multiple ovarian tumors using flow cytometry, ELISA, and transcriptomic assays. This helped us discover that currently available immune therapies like Pembrolizumab do not effectively target specific populations of T and NK cells. By determining this, we have identified BRD1 as an effective immune therapy target in ovarian cancer for which a small molecule therapy does exists. Anti-BRD1 therapies may be effective either alone or in combination with current immune therapies in bolstering a successful anti-tumor immune response in HGSC.

What was the impact on other disciplines?
If there is nothing significant to report during this reporting period, state "Nothing to Report."

Describe how the findings, results, or techniques that were developed or improved, or other products from the project made an impact or are likely to make an impact on other disciplines.

Nothing to Report.

What was the impact on technology transfer?
If there is nothing significant to report during this reporting period, state "Nothing to Report."

Describe ways in which the project made an impact, or is likely to make an impact, on commercial technology or public use, including:
- *transfer of results to entities in government or industry;*
- *instances where the research has led to the initiation of a start-up company; or*
- *adoption of new practices.*

Nothing to Report.

What was the impact on society beyond science and technology?
If there is nothing significant to report during this reporting period, state "Nothing to Report."

Describe how results from the project made an impact, or are likely to make an impact, beyond the bounds of science, engineering, and the academic world on areas such as:
- *improving public knowledge, attitudes, skills, and abilities;*
- *changing behavior, practices, decision making, policies (including regulatory policies), or social actions; or*
- *improving social, economic, civic, or environmental conditions.*

The work so far this year has had a positive impact on using immune therapy to treat ovarian cancer. Previously these therapies have not been effective in ovarian cancer, but based on work in Aim 3, we have now identified critical cellular and mechanistic targets for immune therapy, specifically the protein BRD1, in ovarian cancer which will help identify currently available therapies for these patients and help guide therapeutic design in the future.

5. **CHANGES/PROBLEMS:** *The PD/PI is reminded that the recipient organization is required to obtain prior written approval from the awarding agency grants official whenever there are significant changes in the project or its direction. If not previously reported in writing, provide the following additional information or state, "Nothing to Report," if applicable:*

None.

Actual or anticipated problems or delays and actions or plans to resolve them
Describe problems or delays encountered during the reporting period and actions or plans to resolve them.

The COVID 19 pandemic presented a major obstacle during this reporting period which caused delays. The COVID 19 pandemic caused a tissue banking ban in late February of 2020 at my hospital which was not lifted until late Summer 2020. In addition, surgical operations did not resume at full capacity until Fall 2020. In addition, my institute was shut down from mid-March until June of 2020. For these reasons, I was not able to collect the necessary tissue to generate new organoid lines until Fall 2020. My team is now back in the lab, and we are working hard to complete as much work as we can on Aims 1 and 2 with the organoid lines we generated between 11/19 and 2/20 and now from Fall 2020-April 2021, and we continue to generate new lines with all available tissue. During the shutdown period, Dr. Hill was able to write a manuscript based on the work in this project which has now been accepted (see attached). We have requested a no cost extension for the coming year to complete the work in our approved SOW.

Changes that had a significant impact on expenditures
Describe changes during the reporting period that may have had a significant impact on expenditures, for example, delays in hiring staff or favorable developments that enable meeting objectives at less cost than anticipated.

Please see above. Due to the delayed start due to my human subjects protocol approval, the COVID 19 shutdown, and the COVID19 tissue banking issues, we are behind on expenditures for this year and have requested a one year NCE to complete the proposed work.

Significant changes in use or care of human subjects, vertebrate animals, biohazards, and/or select agents
Describe significant deviations, unexpected outcomes, or changes in approved protocols for the use or care of human subjects, vertebrate animals, biohazards, and/or select agents during the

reporting period. If required, were these changes approved by the applicable institution committee (or equivalent) and reported to the agency? Also specify the applicable Institutional Review Board/Institutional Animal Care and Use Committee approval dates.

Significant changes in use or care of human subjects

None.

Significant changes in use or care of vertebrate animals

None.

Significant changes in use of biohazards and/or select agents

None.

6. **PRODUCTS:** *List any products resulting from the project during the reporting period. If there is nothing to report under a particular item, state "Nothing to Report."*

- **Publications, conference papers, and presentations**
  Report only the major publication(s) resulting from the work under this award.

  Journal publications. *List peer-reviewed articles or papers appearing in scientific, technical, or professional journals. Identify for each publication: Author(s); title; journal; volume: year; page numbers; status of publication (published; accepted, awaiting publication; submitted, under review; other); acknowledgement of federal support (yes/no).*

  Wan, C., Keany, M., Dong, H., Al-Alem, L.F., Pandya, U., Lazo, S., Boehnke, K., Lynch, K.N., Xu, R., Zarrella, D.T., Gu, S., Cejas, P., Lim, K., Long, H., Elias, K., Horowitz, N., Feltmate, C.M., Muto, M.G., Worley, M., Berkowitz, R.S., Matulonis, U.A., Nucci, M.R., Crum, C.P., Rueda, B.R., Brown, M., Liu, X.S., **Hill, S.J.** Enhanced efficacy of simultaneous PD-1 and PD-L1 immune checkpoint blockade in high grade serous ovarian cancer. *Cancer Research*. 2021 Jan 1;81(1):158-173. doi: 10.1158/0008-5472.CAN-20-1674. Epub 2020 Nov 6. Yes.

  Books or other non-periodical, one-time publications. *Report any book, monograph, dissertation, abstract, or the like published as or in a separate publication, rather than a periodical or series. Include any significant publication in the proceedings of a one-time conference or in the report of a one-time study, commission, or the like. Identify for each one-time publication: author(s); title; editor; title of collection, if applicable; bibliographic information; year; type of publication (e.g., book, thesis or dissertation); status of publication (published; accepted, awaiting publication; submitted, under review; other); acknowledgement of federal support (yes/no).*

> None.

Other publications, conference papers and presentations. *Identify any other publications, conference papers and/or presentations not reported above. Specify the status of the publication as noted above. List presentations made during the last year (international, national, local societies, military meetings, etc.). Use an asterisk (*) if presentation produced a manuscript.*

> -7-14-20-Dr. Hill presented this work at the Englander Institute for Precision Medicine at Cornell.
> - 10/14/20-Dr. Hill presented this work for the Society for Functional Precision Medicine
> -04/2021-Dr. Hill was awarded the *Cancer Research* Early Career Award for the above publication funded by this DOD award (https://cancerres.aacrjournals.org/award).

- **Website(s) or other Internet site(s)**
  List the URL for any Internet site(s) that disseminates the results of the research activities. A short description of each site should be provided. It is not necessary to include the publications already specified above in this section.

> None

- **Technologies or techniques**
  Identify technologies or techniques that resulted from the research activities. Describe the technologies or techniques were shared.

> None

- **Inventions, patent applications, and/or licenses**

Identify inventions, patent applications with date, and/or licenses that have resulted from the research. Submission of this information as part of an interim research performance progress report is not a substitute for any other invention reporting required under the terms and conditions of an award.

> None

- **Other Products**
  Identify any other reportable outcomes that were developed under this project. Reportable outcomes are defined as a research result that is or relates to a product, scientific advance, or research tool that makes a meaningful contribution toward the understanding, prevention, diagnosis, prognosis, treatment and /or rehabilitation of a disease, injury or condition, or to improve the quality of life. Examples include:
  - *data or databases;*
  - *physical collections;*
  - *audio or video products;*
  - *software;*
  - *models;*
  - *educational aids or curricula;*
  - *instruments or equipment;*
  - *research material (e.g., Germplasm; cell lines, DNA probes, animal models);*
  - *clinical interventions;*
  - *new business creation; and*
  - *other.*

> Tina's Wish Rising Star Grant-Dr. Hill applied for this award in March of 2019 and received the award in September of 2019.
> NIH 1DP5OD029637-01- Dr. Hill applied for this award in September 2019 and received the award in September 2020.

7. **PARTICIPANTS & OTHER COLLABORATING ORGANIZATIONS**

What individuals have worked on the project?
Provide the following information for: (1) PDs/PIs; and (2) each person who has worked at least one person month per year on the project during the reporting period, regardless of the source of compensation (a person month equals approximately 160 hours of effort). If information is unchanged from a previous submission, provide the name only and indicate "no change".

Example:

Name: *Mary Smith*
Project Role: *Graduate Student*
Researcher Identifier (e.g. ORCID ID): *1234567*
Nearest person month worked: *5*

Contribution to Project: *Ms. Smith has performed work in the area of combined error-control and constrained coding.*
Funding Support: *The Ford Foundation (Complete only if the funding support is provided from other than this award.)*

Name: Sarah Hill

Project Role: PI

Research Identifier: ORCID ID 0000-0002-9199-9459

Nearest person month worked: 3

Contribution to project: Dr. Hill has designed and performed all experiments outlined in the proposal, analyzed all data, and written and submitted a manuscript.

Funding Support: This award, a Tina's Wish Rising Star Grant, previously an AACR AstraZeneca Ovarian Cancer Research Fellowship, previously 1K08CA241093-01A1, and now 1DP5OD029637-01.

Has there been a change in the active other support of the PD/PI(s) or senior/key personnel since the last reporting period?
If there is nothing significant to report during this reporting period, state "Nothing to Report."

If the active support has changed for the PD/PI(s) or senior/key personnel, then describe what the change has been. Changes may occur, for example, if a previously active grant has closed and/or if a previously pending grant is now active. Annotate this information so it is clear what has changed from the previous submission. Submission of other support information is not necessary for pending changes or for changes in the level of effort for active support reported previously. The awarding agency may require prior written approval if a change in active other support significantly impacts the effort on the project that is the subject of the project report.

There have been no changes during the last reporting period.

What other organizations were involved as partners?
If there is nothing significant to report during this reporting period, state "Nothing to Report."

Describe partner organizations – academic institutions, other nonprofits, industrial or commercial firms, state or local governments, schools or school systems, or other organizations (foreign or domestic) – that were involved with the project. Partner organizations may have provided financial or in-kind support, supplied facilities or equipment, collaborated in the research, exchanged personnel, or otherwise contributed.

Provide the following information for each partnership:
<u>*Organization Name:*</u>
<u>*Location of Organization: (if foreign location list country)*</u>
<u>*Partner's contribution to the project*</u> *(identify one or more)*
- *Financial support;*
- *In-kind support (e.g., partner makes software, computers, equipment, etc., available to project staff);*
- *Facilities (e.g., project staff use the partner's facilities for project activities);*
- *Collaboration (e.g., partner's staff work with project staff on the project);*
- *Personnel exchanges (e.g., project staff and/or partner's staff use each other's facilities, work at each other's site); and*
- *Other.*

```
None.
```

8. **SPECIAL REPORTING REQUIREMENTS**

   COLLABORATIVE AWARDS: *For collaborative awards, independent reports are required from BOTH the Initiating Principal Investigator (PI) and the Collaborating/Partnering PI. A duplicative report is acceptable; however, tasks shall be clearly marked with the responsible PI and research site. A report shall be submitted to **https://ers.amedd.army.mil** for each unique award.*

   QUAD CHARTS: *If applicable, the Quad Chart (available on https://www.usamraa.army.mil) should be updated and submitted with attachments.*

9. **APPENDICES:** *Attach all appendices that contain information that supplements, clarifies or supports the text. Examples include original copies of journal articles, reprints of manuscripts and abstracts, a curriculum vitae, patent applications, study questionnaires, and surveys, etc.*

Enhanced Efficacy of Simultaneous PD-1 and PD-L1 Immune Checkpoint Blockade in High-Grade Serous Ovarian Cancer

Changxin Wan[1,2], Matthew P. Keany[3,4], Han Dong[3,5], Linah F. Al-Alem[6,7], Unnati M. Pandya[6,7], Suzan Lazo[3,4], Karsten Boehnke[8], Katherine N. Lynch[4,9], Rui Xu[6,7,10], Dominique T. Zarrella[6], Shengqing Gu[1], Paloma Cejas[4,11], Klothilda Lim[4,11], Henry W. Long[4,11], Kevin M. Elias[7,12], Neil S. Horowitz[7,12], Colleen M. Feltmate[7,12], Michael G. Muto[7,12], Michael J. Worley Jr[7,12], Ross S. Berkowitz[7,12], Ursula A. Matulonis[4,13], Marisa R. Nucci[14,15], Christopher P. Crum[14,15], Bo R. Rueda[6,7,16], Myles Brown[4,9,11], Xiaole Shirley Liu[1,11], and Sarah J. Hill[4,9,14,15]

ABSTRACT

Immune therapies have had limited efficacy in high-grade serous ovarian cancer (HGSC), as the cellular targets and mechanism(s) of action of these agents in HGSC are unknown. Here we performed immune functional and single-cell RNA sequencing transcriptional profiling on novel HGSC organoid/immune cell co-cultures treated with a unique bispecific anti-programmed cell death protein 1 (PD-1)/programmed death-ligand 1 (PD-L1) antibody compared with monospecific anti-PD-1 or anti-PD-L1 controls. Comparing the functions of these agents across all immune cell types in real time identified key immune checkpoint blockade (ICB) targets that have eluded currently available monospecific therapies. The bispecific antibody induced superior cellular state changes in both T and natural killer (NK) cells. It uniquely induced NK cells to transition from inert to more active and cytotoxic phenotypes, implicating NK cells as a key missing component of the current ICB-induced immune response in HGSC. It also induced a subset of CD8 T cells

to transition from naïve to more active and cytotoxic progenitor-exhausted phenotypes post-treatment, revealing the small, previously uncharacterized population of CD8 T cells responding to ICB in HGSC. These state changes were driven partially through bispecific antibody-induced downregulation of the bromodomain-containing protein BRD1. Small-molecule inhibition of BRD1 induced similar state changes *in vitro* and demonstrated efficacy *in vivo*, validating the co-culture results. Our results demonstrate that state changes in both NK and a subset of T cells may be critical in inducing an effective anti-tumor immune response and suggest that immune therapies able to induce such cellular state changes, such as BRD1 inhibitors, may have increased efficacy in HGSC.

Significance: This study indicates that increased efficacy of immune therapies in ovarian cancer is driven by state changes of NK and small subsets of CD8 T cells into active and cytotoxic states.

Introduction

High-grade serous ovarian cancer (HGSC) is the fifth leading cause of cancer death in women in the United States (1). Patients are diagnosed at late stage due to limited early detection methods, and are typically treated with combinations of surgery and chemotherapy (2). Though immune checkpoint blockade (ICB) agents demonstrate success in other solid tumor types, monospecific ICB antibodies exhibit minimal efficacy in HGSC (3, 4). Many theories explore the

contributions of different immune cell types to HGSC outcome and possibly ICB response. Poor HGSC outcomes associate with an increased proportion of tumor-associated macrophages (5). Positive outcomes associate with increased ratios of CD8 T cells to CD4 Tregs (6, 7) and increased fractions of natural killer (NK) cells in ascites (8, 9). Limited mechanistic data explain these findings. On the basis of work in ICB-responsive solid tumor types, it is likely that the quality of the T and NK cells, rather than their quantity, matters in eliciting ICB activity (10, 11).

[1]Department of Data Sciences, Dana-Farber Cancer Institute, Harvard T.H. Chan School of Public Health, Boston, Massachusetts. [2]Program in Computational Biology and Bioinformatics, Duke University, Durham, North Carolina. [3]Department of Cancer Immunology and Virology, Dana-Farber Cancer Institute, Boston, Massachusetts. [4]Department of Medical Oncology, Dana-Farber Cancer Institute, Boston, Massachusetts. [5]Department of Microbiology and Immunology, Harvard Medical School, Boston, Massachusetts. [6]Vincent Center for Reproductive Biology, Department of Obstetrics and Gynecology, Massachusetts General Hospital, Boston, Massachusetts. [7]Obstetrics Gynecology and Reproductive Biology, Harvard Medical School, Boston, Massachusetts. [8]Oncology Translational Research, Eli Lilly and Company, New York, New York. [9]Division of Molecular and Cellular Oncology, Dana-Farber Cancer Institute, Boston, Massachusetts. [10]Department of Internal Medicine, Shaanxi Province Cancer Hospital, Affiliated Hospital of Medical College of Xi'an Jiaotong University, Xi'an, Shaanxi, P.R. China. [11]Center for Functional Cancer Epigenetics, Dana-Farber Cancer Institute, Boston, Massachusetts. [12]Division of Gynecologic Oncology, Department of Obstetrics and Gynecology, Brigham and Women' Hospital, Boston, Massachusetts. [13]Department of Medicine, Brigham and

Women's Hospital, Boston, Massachusetts. [14]Department of Pathology, Brigham and Women's Hospital, Boston, Massachusetts. [15]Department of Pathology, Harvard Medical School, Boston, Massachusetts. [16]Division of Gynecologic Oncology, Department of Obstetrics and Gynecology, Massachusetts General Hospital, Boston, Massachusetts.

In most solid tumors, the tumor microenvironment induces dysfunction in T and possibly NK cells (12, 13). In CD8 T cells, this dysfunction, called "exhaustion," is mediated by stable epigenetic reprogramming producing subsets of differentially functional cells including progenitor-exhausted and terminally exhausted T cells (10, 14, 15). The contribution of naïve versus exhausted CD8 T-cell subsets to ICB response, and the mechanism of NK-cell dysfunction and ICB-triggered response, are still being defined in all solid tumor types, including HGSC (10, 11, 13, 16).

A better understanding of cells critical for ICB response in HGSC and the effect of cell state on their response to ICB agents is needed. Organoid co-cultures containing patient-matched tumor and all intratumoral immune cells represent a human model that can be studied over time using ICB treatments to ask questions about ICB efficacy and mechanism of action (17, 18).

Here we utilize short-term patient-derived HGSC organoid co-cultures containing tumor organoids and the full complement of intratumoral immune cells to functionally assess the mechanism of action of ICB agents in every type of immune cell in the culture. To detect key cellular and mechanistic targets evading current therapies, we compared the action of a novel bispecific anti-programmed cell death protein 1 (PD-1)/programmed death-ligand 1 (PD-L1) ICB antibody (19) with its monospecific anti-PD-1 and anti-PD-L1 controls. We show that the bispecific antibody uniquely induces state changes in NK cells from inert to active states and most strongly induces a state change in CD8 T cells from naïve to cytotoxic progenitor-exhausted states, with neither target previously demonstrated as critical for ICB response in HGSC. We demonstrate that both state changes are driven partially through downregulation of the bromodomain-containing protein BRD1. BRD1 inhibition by a small-molecule inhibitor, BAY-299, recapitulates these state changes for T and NK cells *in vitro* and *in vivo*, and demonstrates efficacy *in vivo*, thereby validating the co-culture results and suggesting BRD1 as a possible immune therapy target. Taken together our data indicate that efficacy of immune therapies in HGSC can be driven by transition of NK-cell and CD8 T-cell subsets into active and cytotoxic states likely through epigenetic changes driven, in part, by BRD1 downregulation or inhibition removing some tumor microenvironment driven dysfunction.

Materials and Methods

For additional and detailed materials and methods, please see Supplementary Materials and Methods.

Patient samples

HGSC tumor tissue was collected from 12 patients undergoing primary debulking surgery at Brigham and Women's Hospital (BWH, Boston, MA) and Dana-Farber Cancer Institute (DFCI, Boston, MA) for organoid co-culture generation and functional testing between December 2019 and April 2020. Tumor tissue from patient 20-22 was obtained under BWH/Partners Institutional Review Board (IRB)–approved discarded tissue protocol 2016P000559. Written informed consent was obtained for the remaining subjects on either BWH/Partners IRB–approved protocol 2016P002819 or DFCI IRB–approved protocol 02-051. All studies in this work were conducted in accordance with the U.S. Common Rule and Belmont Report and approved by the DFCI and BWH/Partners IRBs.

Co-culture generation

Tumors were mechanically dissociated, diluted in DMEM (Life Technologies, catalog no. 11965-092), 10% FBS (Sigma, catalog no. F2442-500), 1% penicillin streptomycin (Life Technologies, catalog no. 15140-122), and 2.5 mg/mL Type II Collagenase (Life Technologies, catalog no. 17101015), and shaken on a horizontal platform for 20 minutes at 37°C. The homogenate was filtered through a 100 μm filter (Corning, catalog no. 352360), pelleted, and washed in 1× Red Blood Cell Lysis Buffer (BioLegend, catalog no. 420301). The cells were then resuspended in DMEM/10% FBS, counted, and diluted to a concentration of 6×10^6 cells (or organoids)/mL in DMEM, 10% FBS, 1% Pen/Strep, and 30 ng/mL of IL2 (PeproTech, catalog no. 200-02) mixed with 15% Matrigel (Corning, catalog no. 356231). This cell suspension was then plated into 48-well plates (USA Scientific, catalog no. CC7672-7548) at 40 μL per well and incubated at 37°C to allow for settling, then drug containing media was added to each well. All drug preparations were prepared in DMEM, 10% FBS, 1% Pen/Strep, and 30 ng/mL of IL2. Drugs included Anti-PD-1 (Selleck, catalog no. A2005), IgGEn Isotype Control (provided by Eli Lilly), anti-PD-L1 (LY3300054), bispecific anti-PD-1/PD-L1 (LY3434172; all antibodies used at 10 μg/mL), and BAY-299 (MedChemExpress, catalog no. HY-107424; used at 1 μmol/L). Co-cultures were harvested 96 hours after plating for all functional assays detailed in the Supplementary Methods.

Single-cell RNA sequencing

Single-cell RNA sequencing (scRNA-seq) experiments were performed by the BWH Single Cell Genomics Core. For scRNA-seq analysis of the organoid co-cultures, viable CD45+ cells from organoid co-cultures were isolated by FACS. Cells were stained with a distinct barcoded antibody (Cell Hashing antibody, TotalSeq-A, BioLegend) as described previously (20). Next, 7,000 cells from each condition were resuspended in 0.4% BSA in PBS at a concentration of 1,000 cells per μL, pooled together, then loaded onto a single lane (Chromium chip, 10× Genomics), followed by encapsulation in a lipid droplet (Single Cell 3′kit V3, 10× Genomics), followed by cDNA and library generation according to the manufacturer's protocol. For the scRNA-seq analysis of the parent tumor, 6,000 viable CD45+ cells and 4,000 CD45− (tumor and stromal cells) were pooled together and resuspended in 0.4% BSA in PBS at a concentration of 1,000 cells per μL. A total of 10,000 cells were loaded onto a single lane (Chromium chip, 10× Genomics), followed by encapsulation in a lipid droplet (Single Cell 3′kit V3, 10× Genomics), followed by cDNA and library generation according to the manufacturer's protocol.

mRNA libraries were sequenced to an average of 50,000 reads per cell and HTO (Cell Hashing antibodies) libraries sequenced to an average of 5,000 reads per cell, both using Illumina Novaseq. Please see Supplementary Materials and Methods for scRNA-seq data analysis methods.

In vivo study

Massachusetts General Hospital Institutional Care and Use Committee protocol 2017N0000236 was used for this study. STOSE cells were cultured and expanded as described previously (21). Twenty 7–9 week-old FVB-N mice obtained from Jackson Labs were intraperitoneally injected with 1×10^7 STOSE cells in 250 μL of PBS. Eighteen days post-injection, mice were weighed and randomized into two arms (10/arm). Randomization was done so that the average weights, weight gained compared with day 0, and SDs were close between the two arms upon starting treatment. The mice were treated with either vehicle [10% NMP (Thermo Fisher Scientific, catalog no. 390682500), 90%PEG400 (Sigma, catalog no. 202398-500G)] or 150 mg/kg BAY-299 (MedChemExpress, HY-107424) by oral gavage once per day for 18 days. Animals were monitored by weight every 3 to

Wan et al.
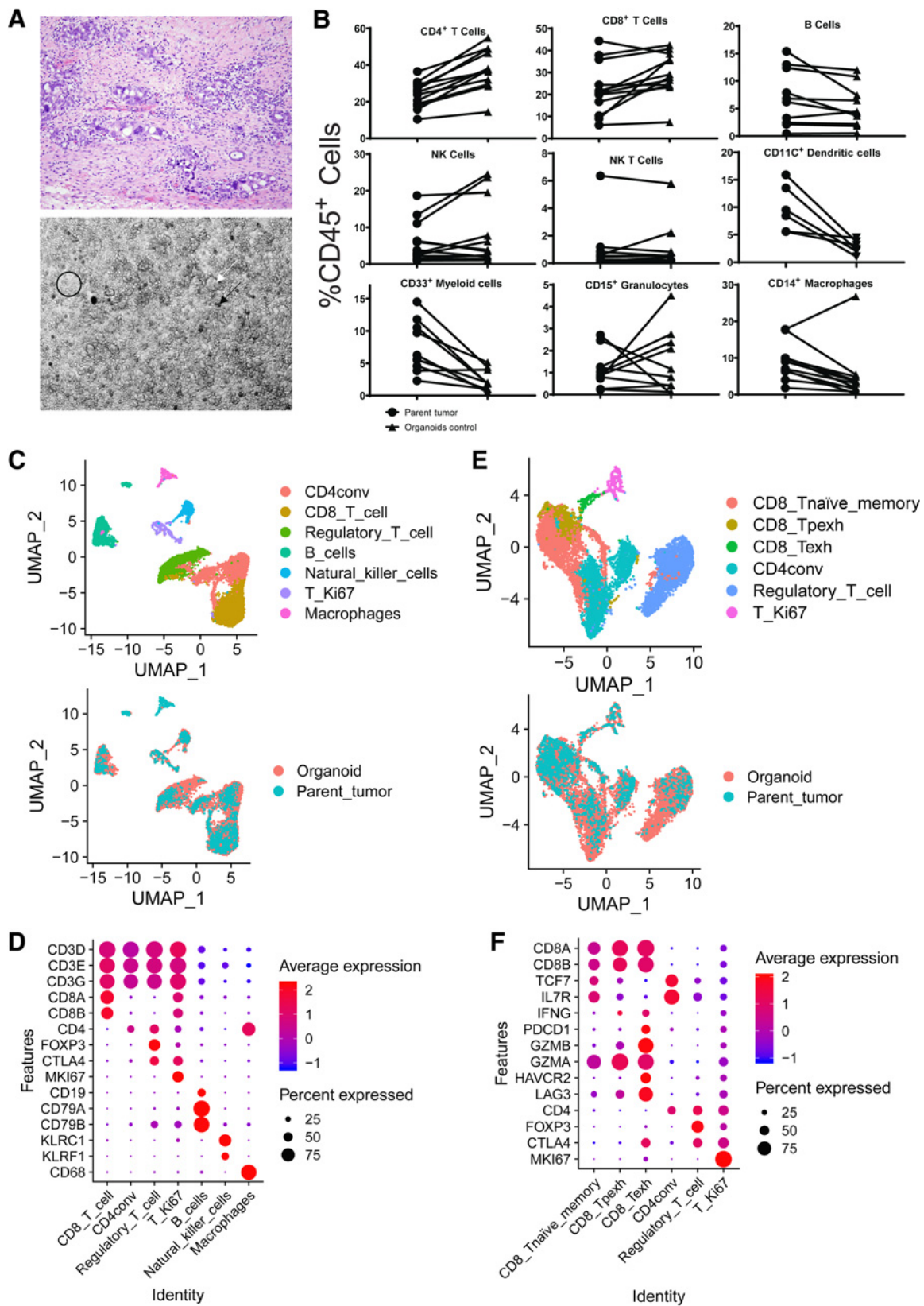
4 days and dosing was adjusted by weight. At the end of the study, mice were euthanized, and ascites and tumors were harvested. Preparation of ascites and tumor cell suspensions for analysis is described in Supplementary Methods.

Accession number

The sequencing data discussed in this study have been deposited in NCBI's Gene Expression Omnibus (GEO) database and are accessible through GEO Series accession number GSE160755.

Results

HGSC organoid–immune cell co-cultures resemble the immune microenvironment of their parent tumors

Short-term co-cultures containing tumor organoids and the full complement of intratumoral immune cells were generated from solid tumors from 12 patients with HGSC, with two sites for 1 patient, making 13 total cultures (**Fig. 1**; Supplementary Fig. S1A). Co-cultures were maintained in a limited growth matrix with minimal growth factor enrichment of the media; experiments occurred immediately after surgery and only lasted 96 hours. These strategies help prevent confounding alterations to the microenvironment, which might occur in longer cultures such as clonal selection of T cells (22, 23). Co-cultures were validated as matching parent tumors through visual, flow cytometry, and sequencing methods.

Bright-field microscopy revealed the co-cultures "look" similar to their parent tumors and contain psammoma body calcifications and groups of tumor spheres permeated by sheets and clusters of immune cells (**Fig. 1A**). Flow cytometry analysis of the parent tumors revealed a significant population of T cells with CD4 cells comprising the majority in most cases, similar to other HGSC studies (24), and revealed a significant population of NK and NK T cells (Supplementary Figs. S1B, S1C and S2A). Flow cytometry comparison of the organoids and parent tumors revealed similar amounts of each immune cell type present in the co-cultures with overall proliferation of T and NK cells and an expected drop in myeloid cells over time (**Fig. 1B**; Supplementary Figs. S1C, S2A and S2B). Significant PD-1, PD-L1, and TIM3 expression was found on relevant immune populations and tumor cells in the co-cultures (Supplementary Figs. S3A–S3D, S4A–S4C and S5A–S5C).

scRNA-seq analysis comparing a single matched parent tumor and control-treated organoid co-culture (20-11) revealed similar annotation of all immune cell types (**Fig. 1C**) defined by standard immune markers (**Fig. 1D**) with a decrease in macrophages mirroring flow cytometry (**Fig. 1B**; Supplementary Fig. S1C). Standard T-cell subsets were detected (**Fig. 1E**) using common subset markers (**Fig. 1F**).

Overall, these flow cytometry and scRNA-seq results confirm that the organoid co-cultures authentically model the parent tumor immune microenvironment.

ICB antibodies reproducibly induce IFNγ production in co-cultures

We next tested the immune activation capacity of ICB antibodies in our system. We sought to compare the efficacy and mechanism of action of a novel bispecific anti-PD-1/PD-L1 antibody (LY3434172; ref. 19) to its monospecific controls, anti-PD-1 (pembrolizumab) and anti-PD-L1 (LY3300054; Supplementary Fig. S6A; ref. 25). Monospecific ICB antibody combinations demonstrate some clinical success (26), but bispecific antibodies are hypothesized to be more effective given their ability to engage two different ICB receptors in close proximity (19, 27). Indeed, compared with monospecific controls, the bispecific anti-PD-1/PD-L1 antibody (LY3434172) has been shown to increase T-cell stimulation in a different *in vitro* system and anti-tumor efficacy *in vivo* in humanized ovarian and other tumor xenograft mouse models through unclear mechanisms (19). On the basis of this, we hypothesized that studying the function of the bispecific anti-PD-1/PD-L1 antibody, compared with controls, in our co-culture system could help dissect critical targets not being affected by available monospecific ICB antibodies.

To measure overall immune response, we performed IFNγ ELISA analysis on media from the 13 co-cultures post-treatment with a physiologic dose of each of the four antibodies individually. Pilot ELISA studies indicated 96 hours post-treatment as the best timepoint (Supplementary Fig. S6B). In six cases, media containing anti-PD-1 and anti-PD-L1 combined or an equivalent amount of IgG (IgG+IgG) was tested to determine whether increased bispecific antibody efficacy was due to an additive effect.

For every tumor analyzed, all three ICB antibodies induced significantly increased IFNγ production compared with the isotype control (**Fig. 2A** and **B**; Supplementary Fig. S6C). The bispecific antibody induced the strongest IFNγ production, not attributable to an additive effect as evidenced by the lower IFNγ production for the anti-PD-1+anti-PD-L1 combination (**Fig. 2A**; Supplementary Fig. S6D).

To compare the aggregate immune activation state of the parent tumors and co-cultures, we generated *IFNG* expression signature scores for each parent tumor as a measure of the bulk tumor immune state, and compared the scores with the co-culture ELISA results as a measure of bulk organoid immune state (**Fig. 2B**; ref. 28). The co-cultures with the highest IFNγ ELISA signals derived from parent tumors with the highest *IFNG* scores (19-107, 19-109, 20-19 omentum), those with medium IFNγ ELISA signals were from parent

Figure 1.

HGSC organoid co-cultures accurately mimic the parent tumors from which they were derived. **A,** Organoid co-cultures (bottom) physically resemble the diverse cellular environment of the parent tumor (top), which includes cancer, stromal, and immune cells. The co-cultures contain tumor spheres (white arrow), clusters of single immune and stromal cells (black circle), and psammoma body calcifications (black arrow). **B,** Flow cytometry analysis for all immune cell types was performed on parent tumors and control-treated organoids. Comparisons of each individual immune cell type between parent tumor (circles) and control-treated organoid co-culture (triangles) as a percentage of viable CD45+ cells are shown. **C–F,** scRNA-seq analysis results comparing the parent tumor and treated organoid co-cultures for patient 20-11. **C,** UMAPs are shown here to demonstrate concordance across all immune cell types between the parent tumor and organoid co-culture. All populations detected are shown on top with a color key on the right, and an overlay of these populations in the parent tumor (blue) and organoid co-cultures (orange) is shown below. **D,** Markers (*y*-axis) used to define each of the individual immune cell populations (*x*-axis) in **C** are shown here along with the expression level in each defined cell type. The average expression level (colors) is shown in the percentage of cells (sphere) expressing each marker for each cell type. **E,** UMAPs are shown here to demonstrate concordance across all T-cell types between the parent tumor and organoid co-culture. All populations detected are shown on top with a color key on the right, and an overlay of these populations in the parent tumor (blue) and organoid co-cultures (orange) is shown below. **F,** Markers (*y*-axis) used to define each of the different T-cell populations (*x*-axis) in **E** are shown here along with the expression level in each defined cell type. The average expression level (colors) is shown in the percentage of cells (sphere) expressing each marker for each cell type. CD8_Tnaïve_memory, naïve and memory CD8 T cells; CD4conv, conventional nonregulatory CD4 T cells; regulatory_T_cell, regulatory CD4 T cells; T_Ki67, proliferating T cells; CD8_Texh, terminally exhausted CD8 T cells; CD8_Tpexh, progenitor-exhausted CD8 T cells.

Wan et al.
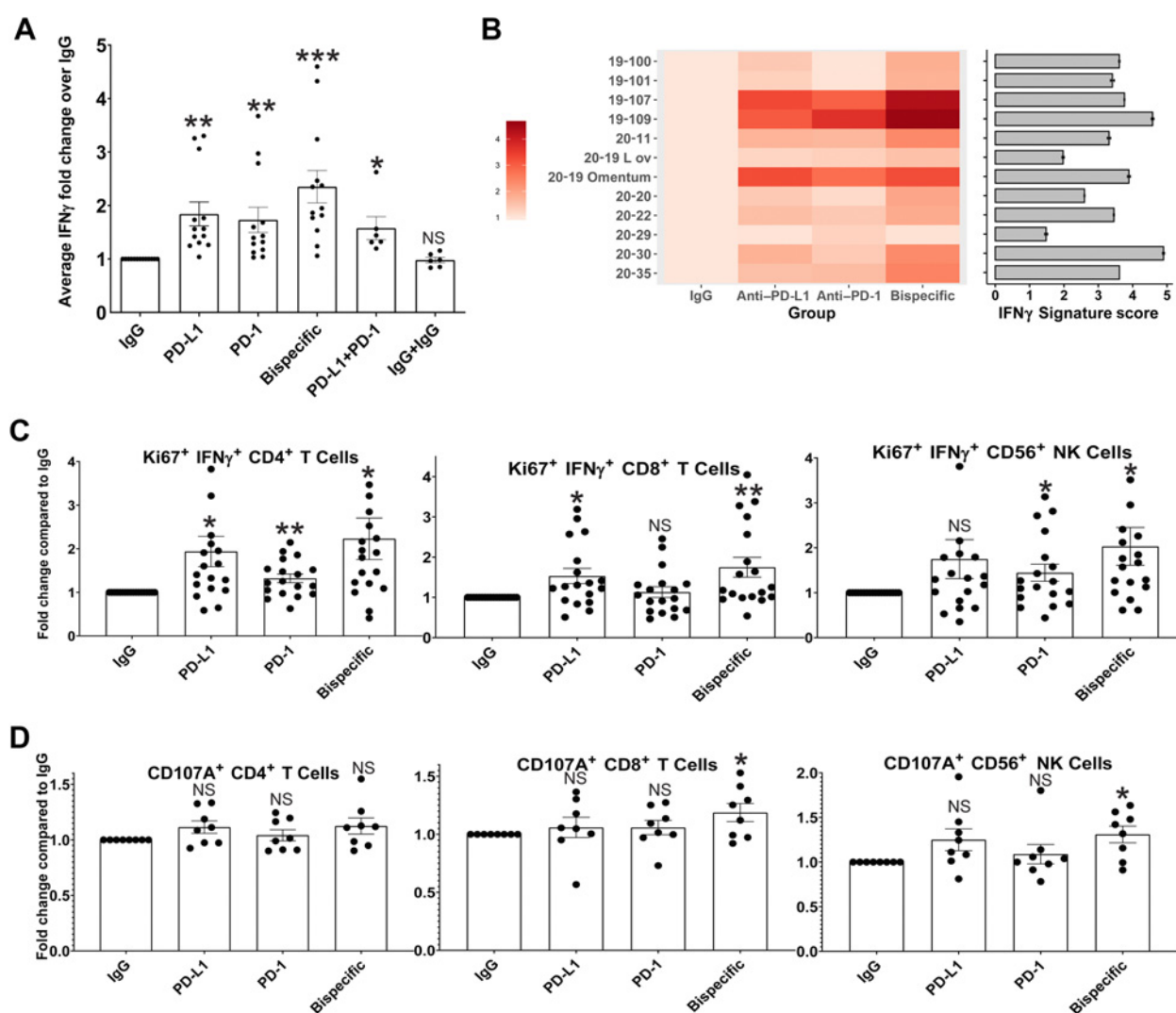
Figure 2.
ICB antibodies induce detectable IFNγ production in proportion to the parent tumor aggregate immune state, increased CD4, CD8, and NK-cell activity, and a killing phenotype in CD8 T and NK cells in HGSC co-cultures. **A,** IFNγ ELISA analysis was performed on media from organoid co-cultures treated with IgG control, anti–PD-L1, anti–PD-1, anti–PD-1/PD-L1 (bispecific), anti–PD-1+anti–PD-L1, and IgG+IgG. Average IFNγ amounts normalized to the IgG control are shown here across all experiments with error bars representing SEM. P values were calculated for all comparisons using a paired t test. Comparisons of key antibodies to the IgG control are shown. *, $P < 0.05$; **, $P < 0.005$; ***, $P < 0.0005$. P values for the significance of other treatment comparisons are shown in Supplementary Fig. S6. **B,** A heatmap is shown for the normalized ELISA results of each individual tumor for IgG, anti–PD-L1, anti–PD-1, and the bispecific antibody. The color code is shown on the left. In addition, bulk RNA-seq was performed on the parent tumors used to generate the co-cultures, and an $IFNG$ signature score was generated. Each tumor was sequenced twice, and the average $IFNG$ score from each parent tumor is shown to the right of the heatmap as a horizontal bar graph with the number score key below. Error bars, SD. **C,** Flow cytometry analysis for IFNγ/Ki67 double-positive CD4$^+$, CD8$^+$, and CD56$^+$ NK cells across treatments normalized to the IgG control. **D,** Flow cytometry analysis for CD107A expression on CD4$^+$, CD8$^+$, and CD56$^+$ NK cells across treatments normalized to the IgG control. *, $P < 0.05$; **, $P < 0.005$; NS, not significant. Error bars, SEM.

tumors with medium scores (19-100, 19-101, 20-11, 20-20, 20-22, and 20-35), and the cultures with low IFNγ ELISA signal derived from the lowest scoring parent tumors (20-29 and 20-19, left ovary; **Fig. 2B**). Patient 20-30 is an outlier with a parent tumor with a high $IFNG$ score but co-cultures with a medium IFNγ signal by ELISA (**Fig. 2B**), potentially due to sampling discrepancies between tissue used for culture and sequencing. Overall, these results indicate that the parent tumor immune activation state is largely matched by the co-cultures and supports the hypothesis that the quality of the immune cells in a tumor rather than the quantity dictate ICB response.

Given our ability to detect immune responses in the co-cultures, we next asked which cells each antibody targets to induce this response.

Different ICB antibodies induce varying degrees of activation in unique immune cell types

Treated organoid co-cultures were analyzed by flow cytometry to determine which cell population(s) each antibody affected by searching for changes in cell numbers and activation markers.

Cell numbers for each lineage were unaffected by the antibodies. There were no changes in T- or NK-cell numbers, CD69$^+$ active T-cell

numbers, or the ratio of CD4:CD8 T cells across all treatments (Supplementary Fig. S7A–S7C). There were no changes in any myeloid cell type except for a small but statistically significant decrease in CD14$^+$ macrophages induced by the bispecific antibody compared with the isotype control (Supplementary Fig. S7A).

We assessed all cell types for markers of proliferation (Ki67), antigen stimulation (IFNγ), and cytotoxic phenotype [granzyme B (GZMB) and CD107A; **Fig. 2C** and **D**; Supplementary Fig. S8A–S8D]. All three ICB antibodies induced a statistically significant increase in antigen-stimulated proliferating Ki67/IFNγ double-positive CD4 and
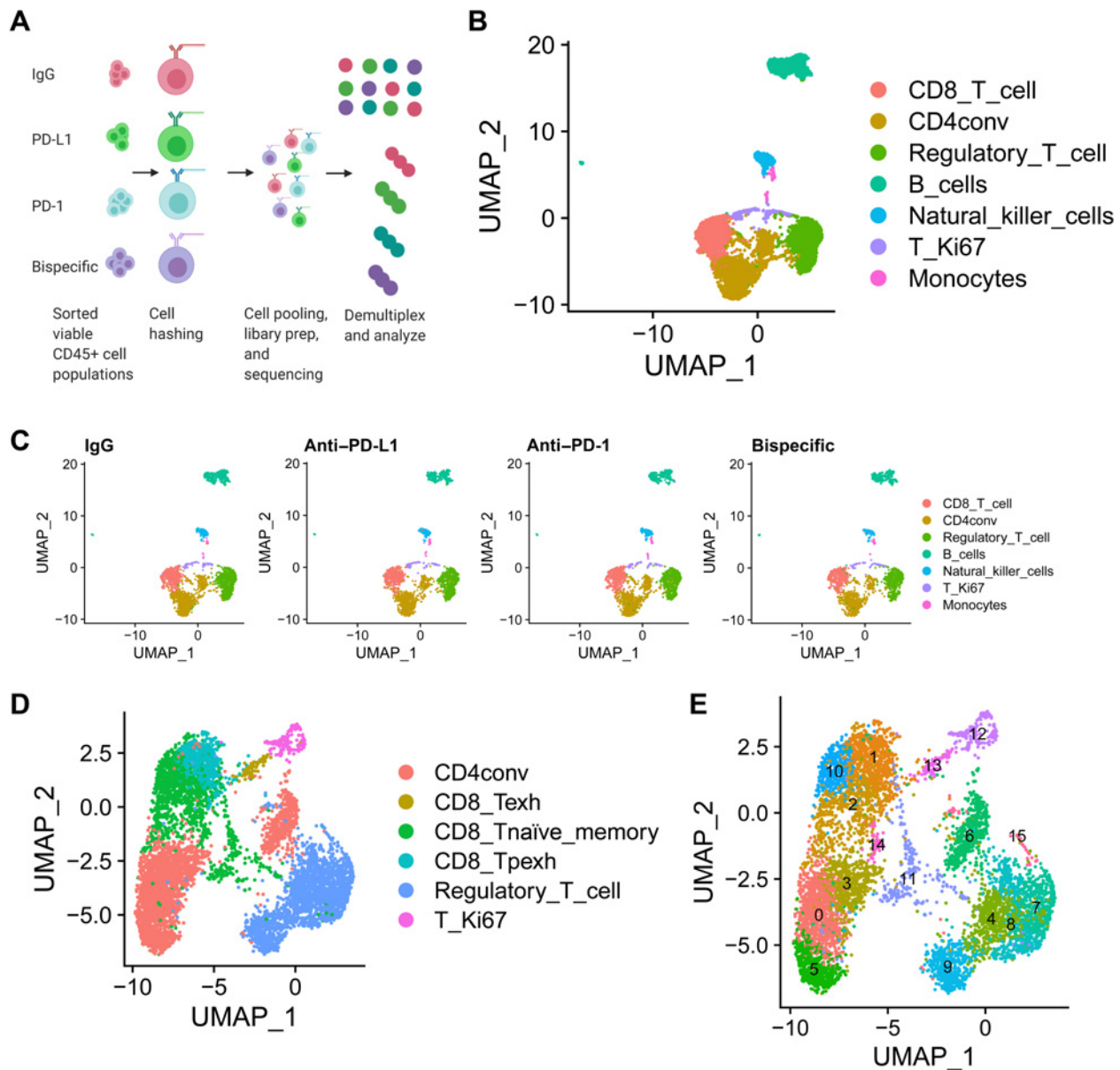
Figure 3.
scRNA-seq analysis of treated organoid co-cultures offers a comprehensive assessment of all immune cell types post-ICB treatment. **A,** Schematic of scRNA-seq experiment. A single organoid co-culture was treated with isotype control, anti-PD-L1, anti-PD-1, or anti-PD-1/PD-L1. Viable CD45$^+$ cells were sorted 96 hours later, hashed with different barcodes for each treatment, mixed in equal proportion, and submitted for 10× genomics library preparation and subsequent sequencing analysis. **B–E,** scRNA-seq analysis comparing results in the organoid co-cultures across treatments. **B,** UMAP demonstrating all immune cells detected in the pool of mixed cells from all treatments from the organoid co-cultures. The color code for each cell type is shown on the right. **C,** UMAPs demonstrating the cells detected in organoid co-cultures from each treatment in the populations in **B** are shown separately to demonstrate equal distribution of all lineages across treatment. Treatment is indicated above the graph and cell type is indicated by a color code on the right. **D** and **E,** UMAPs are shown to demonstrate all T-cell subsets detected across the mixture of cells analyzed across all four treatments and that within each of these subsets there are 15 separate clusters with unique transcriptional states. Cell types are indicated by color codes on the right, and clusters are numbered in **E**. CD4conv, conventional nonregulatory CD4 T cells; T_Ki67, proliferating T cells; CD8_Tpexh, progenitor-exhausted CD8 T cells; CD8_Tnaïve_memory, naïve and memory CD8 T cells; regulatory_T_cell, regulatory CD4 T cells; CD8_Texh, terminally exhausted CD8 T cells.

Wan et al.

CD8 T cells and NK cells, with the bispecific antibody induction the strongest for all three cell types (**Fig. 2C**). Only the bispecific antibody induced an increased percentage of CD107A+ CD8 T cells and NK cells over the IgG control (**Fig. 2D**). Finally, the bispecific antibody induced a small but discernible increase in GZMB-positive CD4 and CD8 T cells and NK cells (Supplementary Fig. S8D). Taken together with the ELISA results, these data indicate that the bispecific antibody induces both an increase in T- and NK-cell activation and cytotoxicity more efficiently than the controls. To better understand the mecha-

nism of ICB antibody-driven immune activation in these cell types, we performed scRNA-seq analysis.

scRNA-seq of treated organoid co-cultures reveals differential expression in all immune lineages after multiple treatment modalities

To study the effects of each ICB antibody on every kind of immune cell in a tumor, we performed scRNA-seq analysis on organoid co-cultures from an untreated HGSC omental metastasis (20-11) 96 hours
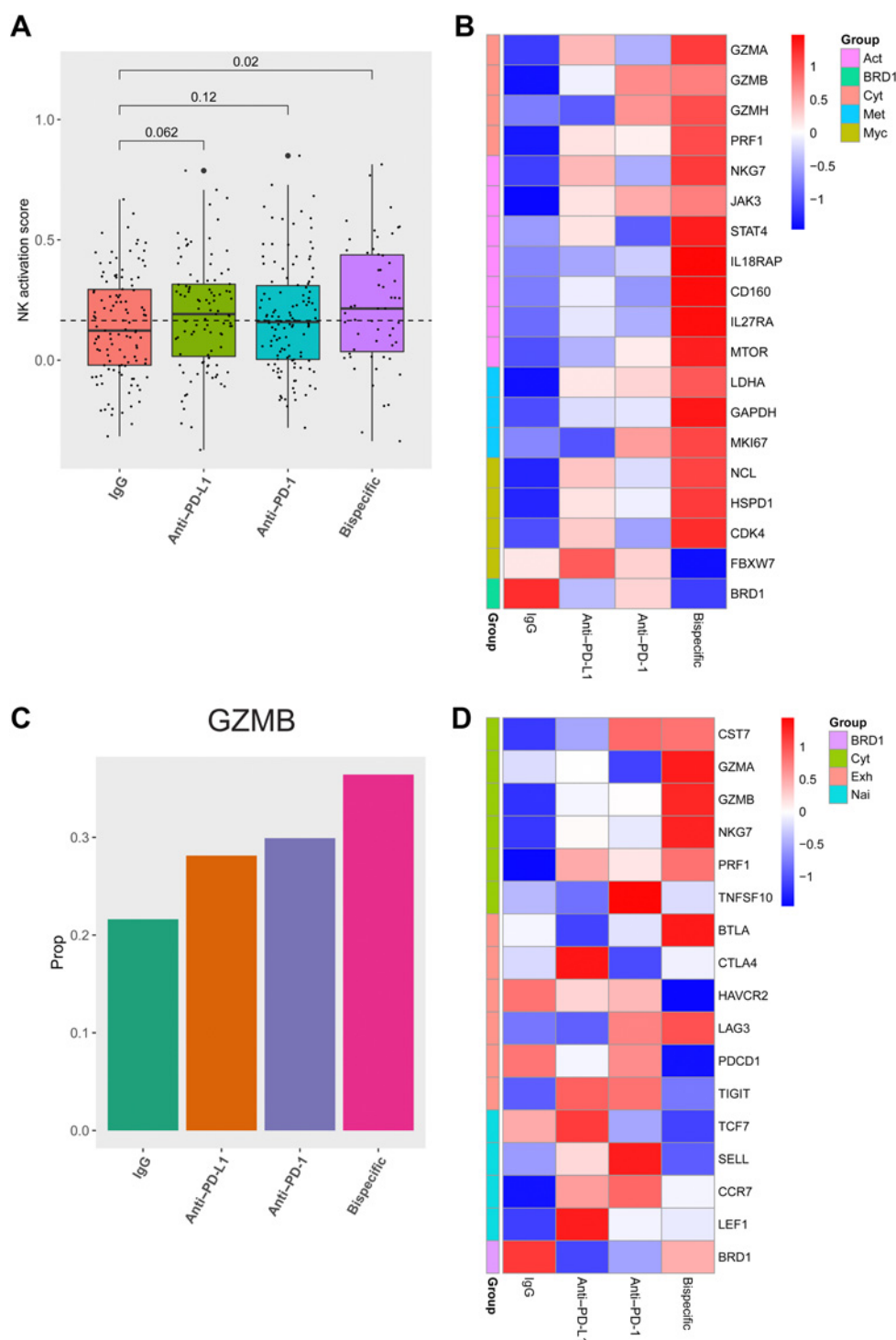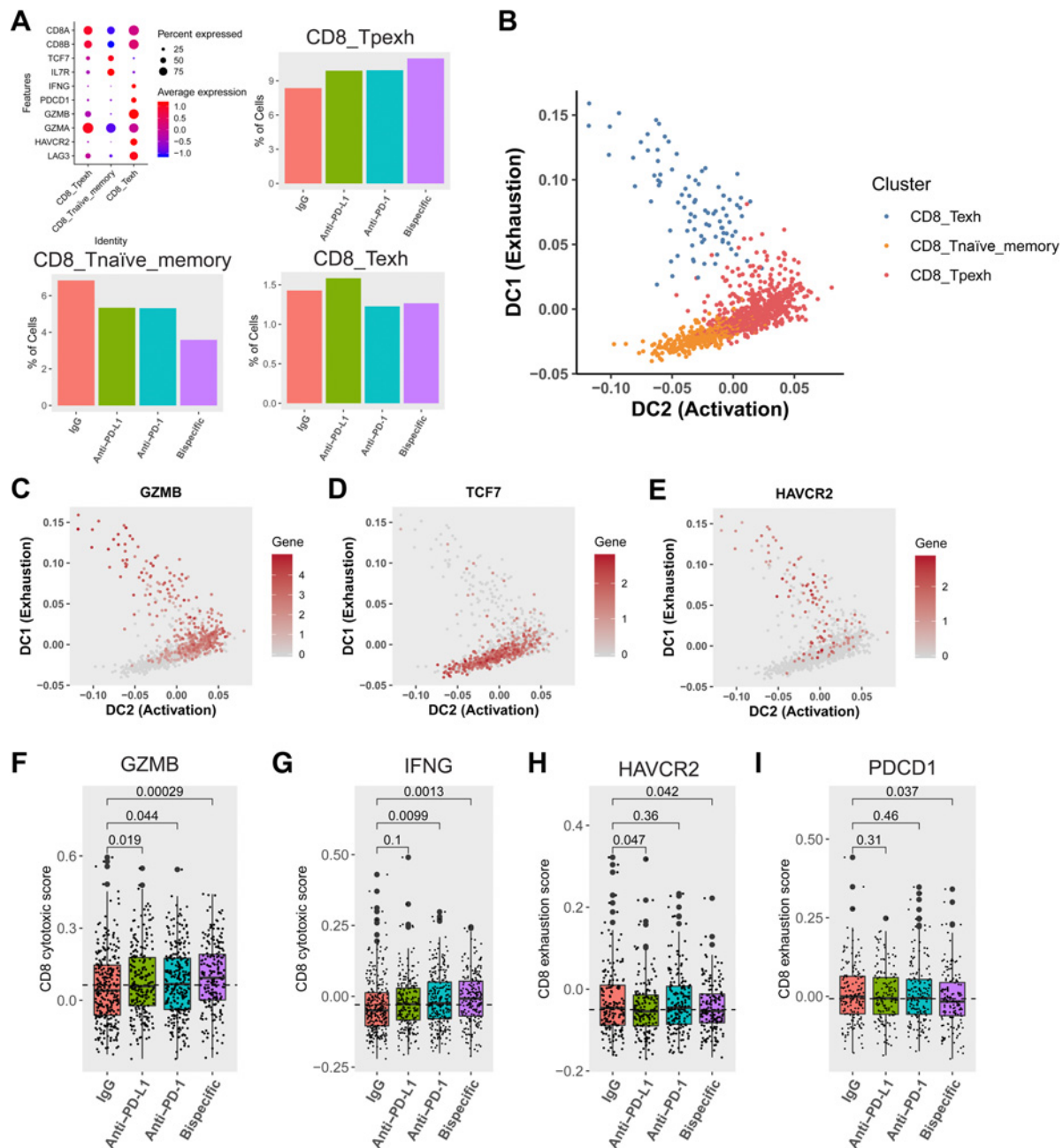

Figure 4.
scRNA-seq analysis reveals that the bispecific antibody induces an increased cytotoxic phenotype in CD8 T cells and NK cells and a decreased exhaustion and naivety phenotype in CD8 T cells. **A,** Activation scores were generated by assessing a panel of 22 genes associated with NK-cell activation. Box plots of the average scores for each treatment are shown, with P values on top generated using a one-tailed t test compared with the isotype control. **B,** A heatmap demonstrating Z scores generated from mean expression in NK cells for genes related to cytotoxicity (cyt; top), activation (act; second from top), metabolism (met; second from bottom), Myc signaling (Myc; third from bottom), and BRD1 (bottom) is shown comparing IgG, anti-PD-L1, anti-PD-1, and the bispecific antibody. **C,** The positive rate of GZMB expression across all treatments in all CD8 T-cell populations combined is shown. **D,** A heatmap demonstrating Z scores generated from mean expression in all CD8 T-cell populations combined for genes related to cytotoxicity (cyt; top), exhaustion (exh; second from top), naivety (nai; second from bottom), and BRD1 (bottom) is shown comparing IgG, anti-PD-L1, anti-PD-1, and the bispecific antibody.

Figure 5.

scRNA-seq analysis reveals state changes in CD8 T cells between distinct subsets. **A,** Definition of and percentage of CD8 T cells in naïve (CD8_Tnaive_memory), progenitor-exhausted (CD8_Tpexh), and terminally exhausted (CD8_Texh) CD8 T-cell groups (mapped in **Fig. 3D** and **E**). On the top left is a bubble map demonstrating markers used to define these three groups. Markers (y-axis) used to define each of the different groups (x-axis) are shown here along with the expression level in each defined cell type. The average expression level (colors) is shown in the percentage of cells (sphere) expressing each marker for each cell type. Bar graphs demonstrating the proportion of CD8 T cells in progenitor-exhausted (top right), naïve (bottom left), and terminally exhausted (bottom right) CD8 T-cell groups across antibody treatments are shown. **B,** Diffusion map demonstrating transition between (i) naïve (orange) and progenitor-exhausted (red) cells, and (ii) terminally exhausted (blue) and progenitor-exhausted (red) cells over pseudotime. The x-axis represents increasing activation, and the y-axis represents increasing exhaustion. The color code for the different clusters/subgroups is shown on the top right. **C–E,** Diffusion maps demonstrating transition between naïve and progenitor-exhausted cells and terminally exhausted and progenitor-exhausted cells (mapped in **B**) over pseudotime for the activation marker *GZMB* (**C**), the naivety marker *TCF7* (**D**), and the exhaustion marker *HAVCR2* (TIM3; **E**). The x-axis represents increasing activation, and the y-axis represents increasing exhaustion. The color code for gene expression level is shown on the right. **F** and **G,** Activation scores were generated by assessing a panel of 50 genes associated with *GZMB* (**F**) or *IFNG* expression (**G**) in CD8 T cells in naïve and progenitor-exhausted CD8 T cells. Box plots of the average scores for each treatment are shown with P values compared with the IgG control for *GZMB* (**F**) and *IFNG* (**G**). **H** and **I,** Exhaustion scores were generated by assessing a panel of 50 genes associated with *HAVCR2* (TIM3; **H**) expression or *PDCD1* (PD-1; **I**) expression in CD8 T cells in both naïve and progenitor-exhausted cells. Box plots of the average scores for each treatment are shown with P values compared with the control for *HAVCR2* (**H**) and *PDCD1* (**I**). All P values were generated using a one-tailed t test.

Wan et al.
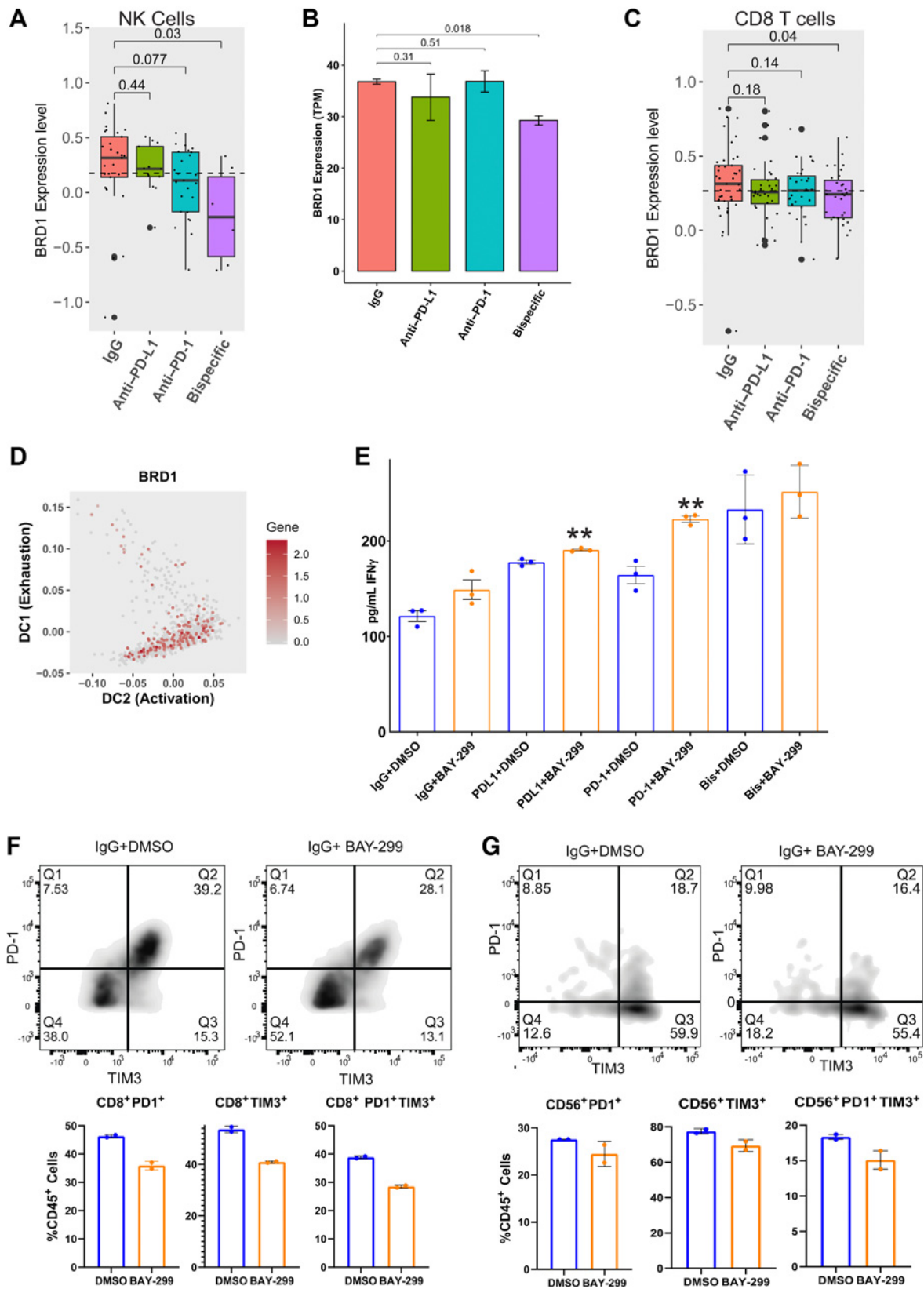
post-treatment, with isotype control, anti-PD-1, anti-PD-L1, or the bispecific antibody (**Fig. 3A**). Viable CD45$^+$ cells from each treatment were sorted, hashed (20), harvested for library preparation, and sequenced (**Fig. 3A**).

Analysis and cell type annotation of the pooled samples revealed every immune cell type was detectable (**Fig. 3B**) with equal numbers of each immune cell type present across all four treatment groups (**Fig. 3C**). All T-cell subtypes were present (**Fig. 3D**), and unsupervised clustering by Seurat (29) identified 15 unique T-cell subsets/clusters each with distinct transcriptional states (**Fig. 3E**). All immune cell types showed differential expression across treatments (Supplementary Figs. S9A–S9N, S10A–S10D and S11A–S11K; Supplementary Tables S1–S4).

Gene expression analysis reveals increased cytotoxicity in T and NK cells and decreased exhaustion in T cells induced most strongly by the bispecific antibody

We analyzed CD8 T and NK cells for activity or cytotoxicity marker expression. For NK cells, we analyzed expression across a panel of 22 NK-cell activation genes to generate activation scores for each treatment (**Fig. 4A**; Supplementary Table S5; ref. 30). The highest and only statistically significant score was for the bispecific antibody compared with the isotype control. Furthermore, we analyzed expression of genes associated with NK-cell cytotoxicity, activation, metabolism, and Myc signaling (30–33). Upregulation of c-Myc or its targets and down-regulation of Myc degraders (FBXW7) cause NK-cell expansion and metabolic activation (32, 34). The bispecific antibody induced the greatest increase in expression of all cytotoxicity, activation, metabolism, and Myc targets and the strongest decrease of *FBXW7* (**Fig. 4B**). Bispecific antibody upregulation of *GZMB* was independently verified in sorted NK cells from a different patient's treated organoid co-cultures (Supplementary Fig. S10D). These results suggest a state change from inert to highly active. Neither monospecific antibody induced NK-cell activation, suggesting that NK-cell activation is a unique bispecific antibody target.

Gene expression analysis of bulk CD8 T cells revealed that all ICB agents induced *GZMB* expression, most strongly the bispecific antibody (**Fig. 4C**), validating flow cytometry findings (Supplementary Fig. S8D). The bispecific antibody induced a larger increase in expression of multiple cytotoxicity markers, including *GZMA, GZMB*, and *PRF1* (**Fig. 4D**). *GZMB* upregulation was validated in CD8 T cells

sorted from organoid co-cultures from a different patient (Supplementary Fig. S11G). In addition, the bispecific antibody induced an overall decrease in expression of a subset of exhaustion markers (*PDCD1* = PD-1 and *HAVCR2* = TIM3) and naïve T-cell markers (*TCF7* and *SELL*), suggesting a shift of the CD8 T cells from naïve and exhausted states to active (**Fig. 4D**). However, shifts in the bulk CD8 T-cell analysis were small and sometimes inconsistent across functional groups (**Fig. 4D**). In other tumor types, small subsets of CD8 T cells respond to ICB therapies (10, 11), prompting us to reexamine activation and exhaustion marker expression in each CD8 subset to determine the reason for the smaller shifts we were observing in the bulk CD8 T-cell analysis and if this also occurs in HGSC (**Fig. 4C** and **D**).

CD8 T-cell trajectory analysis suggests a state transition induced by ICB antibodies

To identify which CD8 T cells respond to ICB agents, we focused on three subsets including naïve, progenitor exhausted, and terminally exhausted, all defined by varying expression of activation, naivety, and exhaustion markers (**Fig. 5A**; refs. 10, 11). Examination of these subsets across the four treatment groups reveals (i) an increase in progenitor exhausted and a decrease in naïve groups both most prominent after bispecific antibody treatment, and (ii) small decreases within the terminally exhausted group after anti-PD-1 and bispecific antibody treatment (**Fig. 5A**). This suggested a state transition within these groups in response to ICB (10, 11).

To define the direction of the dynamic state shifts between these three CD8 T-cell groups in response to treatment, we utilized diffusion maps of activation (*GZMB, PRF1, IFNG*), naivety (*TCF7, SELL*), and exhaustion [*HAVCR2* (TIM3)] markers ordered in pseudotime (**Fig. 5B–E**; Supplementary Fig. S11H–S11J; refs. 11, 35). The activation markers increase between naive and progenitor exhausted, and terminally exhausted and progenitor-exhausted cells (**Fig. 5B**; Supplementary Fig. S11H and S11J), the naivety markers decrease from naïve into progenitor-exhausted cells (**Fig. 5D**; Supplementary Fig. S11I), and the exhaustion markers decrease from terminally exhausted into progenitor-exhausted cells and from progenitor exhausted into naïve cells (**Fig. 5E**). These transitions are most significantly induced by the bispecific antibody (**Fig. 5A**). Overall, this suggests that naïve CD8 T cells might give rise to the progenitor-exhausted active subset, and that some terminally exhausted cells shift

---

Figure 6.

The bispecific antibody acts, in part, through strongly depleting *BRD1* expression, leading to increased immune activity through activation and state changes in T and NK cells. **A,** *BRD1* expression was analyzed across different treatment groups from the scRNA-seq experiment (**Fig. 3**) for NK cells. Bar graph demonstrating the expression level of *BRD1* in NK cells for each ICB antibody compared with the IgG control. *P* values were generated using a one-tailed *t* test. **B,** To verify the *BRD1* depletion induced by the bispecific antibody in NK cells, another organoid co-culture from an untreated patient with HGSC (20–35) was treated with isotype control, anti-PD-1, anti-PD-L1, or anti-PD-1/PD-L1. NK cells were sorted from the treated cultures at the 96-hour timepoint and sent for bulk RNA-seq. The *BRD1* expression across treatments is shown here as transcripts per million (TPM). *P* values were generated using a one-tailed *t* test. **C,** *BRD1* expression was analyzed across different treatment groups from the scRNA-seq experiment (**Fig. 3**) for the naïve and progenitor-exhausted CD8 T-cell subgroups combined. Shown here is a bar graph demonstrating the expression level of *BRD1* in the combined ICB-responsive naïve and progenitor-exhausted CD8 T cells compared with the IgG control. *P* values were generated using a one-tailed *t* test. **D,** Diffusion map demonstrating *BRD1* expression in CD8 T-cell subgroups transitioning between naïve and progenitor-exhausted CD8s and terminally exhausted and progenitor-exhausted CD8s (mapped in **Fig. 5B**). The *x*-axis represents increasing activation, and the *y*-axis represents increasing exhaustion. The color code for gene expression level is shown on the right. **E,** The same organoid co-culture from **B** (20–35) was treated with isotype control, anti-PD-1, anti-PD-L1, or anti-PD-1/PD-L1 combined with either DMSO (blue) or the BRD1 inhibitor BAY-299 (orange). The co-culture media supernatants underwent IFNγ ELISA analysis, shown here as the average pg/mL of IFNγ for the treatment, with error bars representing SE. **, *P* < 0.005. **F and G,** The treated organoid co-cultures from **B** and **E** underwent flow cytometry analysis for PD-1 and TIM3 single-positive and double-positive cells. Only the IgG and PD-L1–treated cultures could be analyzed here because the anti-PD-1 and bispecific antibody–treated co-cultures showed decreased PD-1 due to the treatment antibody blocking the flow antibody. **F,** The flow quadrant plots for IgG+DMSO and IgG+BAY-299 are shown for CD8 T cells on the top. PD-1 is on the *y*-axis and TIM3 is on the *x*-axis. The percentage of PD-1 (Q1) and TIM3 (Q3) single-positive and double-positive (Q2) CD8 T cells is shown on the bottom as a percent of CD45$^+$ cells. Error bars, SE across two replicates. **G,** The flow quadrant plots for IgG+DMSO and IgG+BAY-299 are shown for NK cells on the top. PD-1 is on the *y*-axis and TIM3 is on the *x*-axis. The percentage of PD-1 (Q1) and TIM3 (Q3) single-positive and double-positive (Q2) NK cells is shown on the bottom as a percent of CD45$^+$ cells. Error bars, SE across two replicates.

Wan et al.
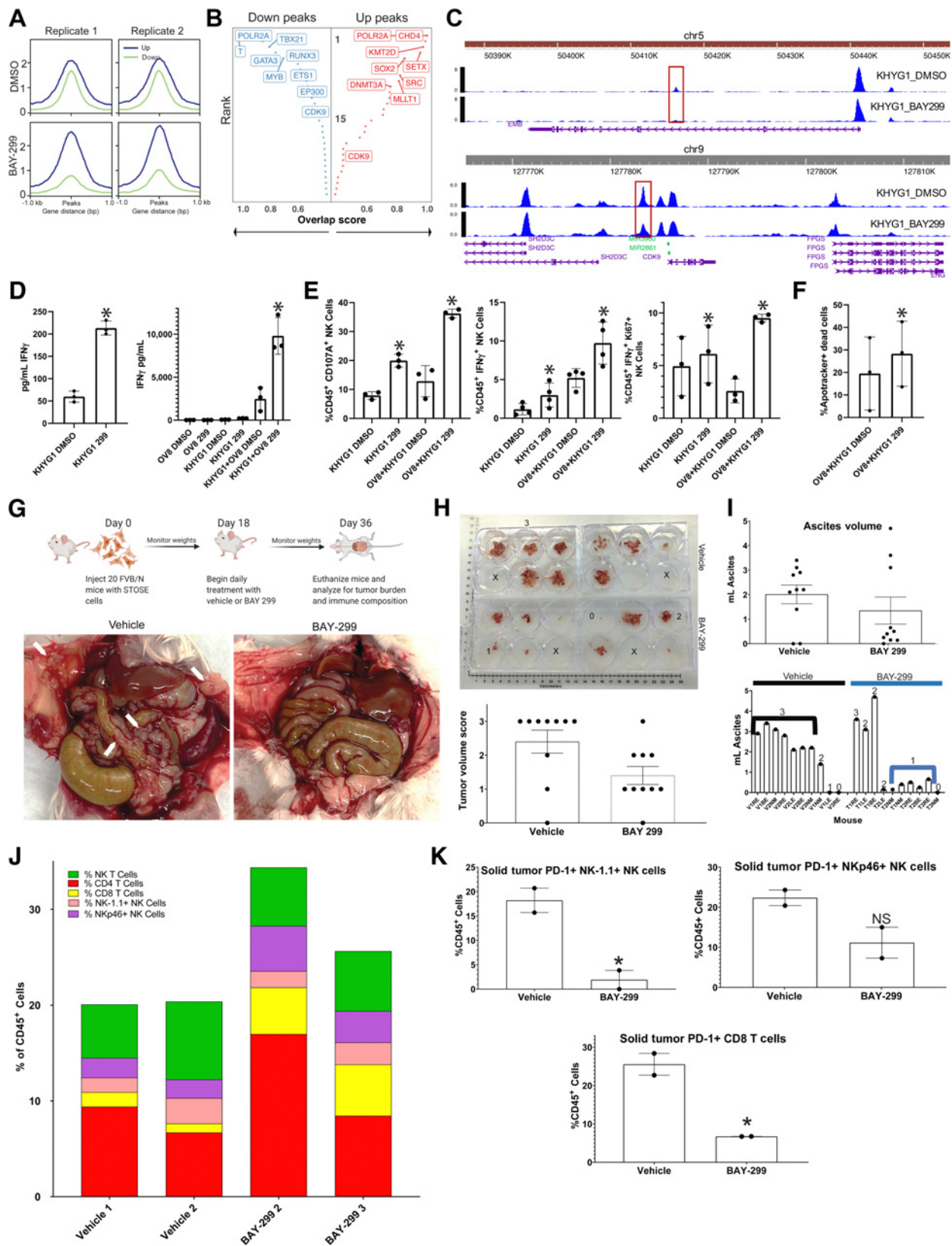
to the more active progenitor-exhausted state (**Fig. 5B**), both changes observed in other tumor types in response to ICB (10, 11).

Having defined the naïve and progenitor-exhausted groups as the ICB responders, we reexamined the exhaustion and activation marker gene panels, which revealed only small shifts in the bulk CD8 T cells (**Fig. 4D**). By assessing expression of the top 50 genes associated with either *GZMB* (**Fig. 5F**) or *IFNG* (**Fig. 5G**) in the combined progenitor-exhausted and naïve CD8 T-cell groups, we generated activation scores for these cells across treatments and found the largest statistically significant increases were for the bispecific antibody over the isotype control for both *GZMB* and *IFNG* (**Fig. 5F** and **G**). Similarly, we assessed expression across the top 50 genes associated with either *HAVCR2* (TIM3; **Fig. 5H**) or *PDCD1* (PD-1; **Fig. 5I**) in the same combined CD8 groups to generate exhaustion scores across treatments. We found a statistically significant decrease for anti-PD-L1 and the bispecific antibody over the isotype control for *HAVCR2*-associated genes (**Fig. 5H**) and for the bispecific antibody for *PDCD1*-associated genes (**Fig. 5I**). These results validated our findings regarding the decreased exhaustion and overall active state changes the bispecific antibody in particular induced within these CD8 groups (**Fig. 5B**).

We next sought to determine the mechanism of how the bispecific and other ICB antibodies induce these changes.

The bispecific antibody induces decreased T- and NK-cell exhaustion by downregulating BRD1 expression in immune cells

We examined the differentially expressed genes for the bispecific antibody compared with the controls in the CD8 T- and NK-cell populations, searching for cell state control genes with small-molecule therapies. We focused on the bromodomain-containing protein BRD1, which is known to regulate CD8 T and other cell development (36, 37) and has a small-molecule inhibitor, BAY-299 (38). *BRD1* expression was downregulated by the bispecific antibody in NK cells in the scRNA-seq data (**Figs. 4B** and **6A**; Supplementary Fig. S10A;

Supplementary Table S4) and in bulk RNA seq of sorted NK cells from treated organoid co-cultures from a different patient (**Fig. 6B**). All ICB antibodies induced a decrease in *BRD1* expression in bulk (**Fig. 4D**) and combined ICB-responding progenitor-exhausted and naïve CD8 T cells (**Fig. 6C**), and by anti-PD-L1 in terminally exhausted CD8 T cells (Supplementary Fig. S11K). In diffusion analysis over pseudotime, *BRD1* expression decreased from naïve into progenitor exhausted cells and progenitor into terminally exhausted cells (**Fig. 6D**), suggesting the depletion was leading to an increase in activation and decrease in exhaustion. On the basis of these data, we hypothesized that BRD1 may negatively regulate T and NK cells and that BRD1 downregulation or inhibition may lead to enhanced antitumor immune function.

We examined *BRD1* expression in Tumor Immune Estimation Resource, a compilation of expression profiling of immune cells across multiple tumor types to determine whether *BRD1* expression in HGSCs *in vivo* correlates with immune cell inhibition (39). We found that *BRD1* expression is low in tumor cells and high in immune cells in HGSC (Supplementary Fig. S12). High *BRD1* expression correlated with significant downregulation of T- and NK-cell activity markers (*GZMA, GZMB, IFNG,* and *NKG7*) and upregulation of the naïve T-cell marker *TCF7* supporting our hypothesis that BRD1 is a negative regulator of T- and NK-cell activity (Supplementary Fig. S12).

To confirm that *BRD1* is a negative immune regulatory gene, we tested the BRD1 inhibitor BAY-299 (38) in HGSC organoid co-cultures. We observed that BAY-299 combined with isotype control, anti-PD-1, or anti-PD-L1 leads to a statistically significant increase in IFNγ levels over any antibody alone, indicating increased immune activation (**Fig. 6E**). BAY-299 addition generated only a small increase in IFNγ levels over bispecific antibody alone (**Fig. 6E**), as expected, given the bispecific antibody-induced depletion of BRD1 in key cell types (**Fig. 6A–C**).

Given the state transitions induced by the bispecific antibody (**Figs. 4** and **5**), we wondered whether BRD1 inhibition caused

---

Figure 7.

A BRD1 inhibitor causes increased anti-tumor immunity in HGSC by altering immune cell chromatin state. **A,** ATAC-seq was performed in duplicate on KHYG1 cells treated with either vehicle or BAY-299. Aggregated reads within 1 kb on either side of center for up (blue) and down (green) differentially accessible chromatin sites for the two replicates for DMSO (top) and BAY-299 (bottom)-treated cells are shown here. **B,** The transcription factors associated with the most strongly altered up (right; red) and down (left; blue) peaks. The y-axis represents rank of the transcription factor from 1 (highest rank at top) to 30 (lowest rank at bottom) for number of overlapping sites, and the x-axis represents the overlap score increasing from left to right for up peaks and right to left for down peaks. Highest ranking TFs are on the top left for down peaks and top right for up peaks. **C,** Chromatin peaks surrounding and within the *EMB* (top) and *CDK9* (bottom) genomic locus for DMSO-treated KHYG1 cells (top in each panel) and BAY-299–treated KHYG1 cells (bottom in each panel). The taller the peak, the more open the chromatin. The scale for peak size is on the y-axis and the x-axis represents location in the genome. **D,** KHYG1 cells treated with DMSO vehicle or BAY-299 (299) were plated either alone or in co-culture with OVCAR8 (OV8) tumor cells, and the media was subsequently tested for IFNγ presence by ELISA. Bar graphs for the ELISA for KHYG1 cells alone is shown on the left and for the co-cultures on the right. Error bars, SD between three replicates of the experiment. *, P < 0.05 using a paired t test. **E,** KHYG1 cells treated with vehicle DMSO or BAY-299 (299) were plated either alone or in co-culture with OVCAR8 (OV8) tumor cells, and the cultures were analyzed by flow cytometry for NK cell CD107A expression (left), IFNγ expression (middle), and IFNγ/Ki67coexpression (right). Error bars, SD between 3–4 replicates. *, P < 0.05 using a paired t test. **F,** KHYG1 cells treated with DMSO vehicle or BAY-299 (299) were plated in co-culture with OVCAR8 (OV8) tumor cells, and 6 hours later the OVCAR8 cells were analyzed for apoptotic death. The percentage of nonviable apoptotic cells (Apotracker+ Dead Cells) from three separate experiments is shown here for each group, with error bars representing SD. *, P < 0.05 using a paired t test. **G,** Top, a schematic of the *in vivo* experiment is shown. Bottom, gross images of the tumor burden in vehicle and BAY-299–treated mice are shown with white arrows pointing to solid tumor deposits on the peritoneum and bowel. The animals shown are representative of the most common tumor burden levels in each group. **H,** Top, grossly visible solid tumors were dissected from each mouse in each group, and a photo of tumor volume is shown. Solid tumors from each animal were placed in a well of a 6-well plate for visual volume scoring. A 3 represents high tumor burden; 2, medium tumor burden; 1, limited tumor burden; 0, no tumor burden. Numbers are placed in representative 3, 2, 1, and 0 wells, and an X is placed in empty wells. Bottom, the tumor volume scores are shown for all 10 animals per group in a bar graph, with error bars representing SEM. **I,** Ascites was aspirated from each animal and the volume measured. Top, a bar graph of the ascites volumes for all animals in each group, with the error bars representing SEM. Bottom, the individual animal ascites volumes with the numeric tumor volume score for each animal over the volume bar. Black and blue lines mark the vehicle and treatment groups most common volume and tumor burdens. **J,** Solid tumors were harvested from each animal in both the vehicle and treatment groups. For each treatment group, the tumors for 3–4 animals were combined. There were only enough cells from two combined groups each for vehicle and BAY-299 to perform flow analysis. The single-cell suspensions of the solid tumors were analyzed for T and NK composition, which is shown here. Each color represents a cell type and each bar represents a group. The color code is at the top left. **K,** PD-1 expression was analyzed in both solid tumor treatment groups on NK-1.1+ NK cells (top left), NKp46+ NK cells (top right), and CD8 T cells (bottom), and the percent of PD-1+ T or NK cells for each treatment group is shown here as a percentage of CD45+ cells. Error bars, SD. *, P < 0.05 generated using an unpaired t test; NS, not significant with an unpaired t test.

---

increased immune efficacy through a cell state change. We examined exhaustion markers TIM3 and PD-1 (40) on T- and NK-cell populations from HGSC organoid co-cultures treated with our ICB antibody panel ± BAY-299 by flow cytometry. BAY-299 treatment decreased the number of TIM3 or PD-1 single-positive and TIM3/PD-1 double-positive CD3, CD4, and CD8 T cells and NK cells (**Fig. 6F** and **G**; Supplementary Fig. S13A and S13B), indicating that BRD1 inhibition may indeed be leading to a cell state change from an exhausted to an active phenotype as observed for all ICB antibodies, most significantly the bispecific antibody (**Figs. 4–6**). Thus, an underlying mechanism of action for the increased efficacy of the bispecific antibody is potentially an induction of *BRD1* depletion in NK and T cells, promoting active states (**Figs. 5** and **6**). The next question was how BRD1 depletion induces this state change and if it increases tumor cell killing.

BRD1 inhibition leads to increased NK-cell activation and tumor cell killing partially through altering chromatin access for key immune transcription factors

To study the mechanism of BRD1 inhibition–induced immune cell state changes, we applied BAY-299 to an NK-cell line, KHYG1 (41). BAY-299 caused a small decrease in BRD1 protein levels in the KHYG1 cells after a 96-hour exposure (Supplementary Fig. S14A). In a growth rate–corrected sensitivity analysis, BAY-299 was not overtly toxic to HGSC tumor, NK-, or T-cell or HGSC organoid lines (Supplementary Fig. S14B; ref. 42).

Assay for transposase-accessible chromatin using sequencing (ATAC-seq) analysis of BAY-299–treated KHYG1 cells revealed significant alterations to chromatin accessibility across the genome (**Fig. 7A**; Supplementary Fig. S14C). The major chromatin alterations showed significant overlap with binding sites for key NK-cell development regulatory transcription factors such as GATA3, TBX21, and TBXT, which were all associated with down peaks (**Fig. 7B**; ref. 43). Several genes linked to these transcription factors with important biological functions were in altered peaks. For example, BAY-299 caused alterations in the chromatin accessibility of the promoter region of *CDK9* (**Fig. 7C**, bottom). CDK9 is, in part, recruited to immune genomic loci by TBX21 as part of the PTef-b complex (44), and CDK9 inhibition allows global reactivation of epigenetically silenced genes, leading to increased IFNγ activity and sensitivity to ICB agents in tumor cells (45). In addition, BAY-299 reduces chromatin accessibility of *EMB* (**Fig. 7C**, top), another TBX21-regulated gene recently identified as a marker of immature NK cells and as part of an immature NK-cell signature (46). Taken together, these findings suggest that a possible BRD1 inhibitor mechanism of action is altering chromatin accessibility for major NK-cell regulatory transcription factors at key immune modulatory genes to allow for a mature (*EMB*) active and cytotoxic (*CDK9*) state.

To test for this possibility, we functionally assessed BAY-299–treated NK-tumor cell co-cultures. BAY-299 led to increased IFNγ production by the NK cells alone and at even higher levels when in co-culture with the HGSC cell line OVCAR8 or organoid line 17-116 (47), indicating increased immune activity (**Fig. 7D**; Supplementary Fig. S14D). Accordingly, paired flow cytometry analysis of the NK cells after BAY-299 treatment either alone or in co-culture demonstrated increased IFNγ⁺, Ki67⁺/IFNγ⁺ double-positive cells, and CD107A⁺ NK cells, more pronounced when these cells were cultured with OVCAR8 or organoid tumor cells (**Fig. 7E**; Supplementary Fig. S14E). Finally, BAY-299 increased tumor cell killing over vehicle in KHYG1 and OVCAR8 cell co-cultures (**Fig. 7F**). Altogether, these results indicate that BAY-299 induced chromatin remodeling causes a more cytotoxic and active state in NK cells

in vitro and begs the question of whether BAY-299 can lead to enhanced anti-tumor killing by NK and possibly other cytotoxic immune cells *in vivo*.

BRD1 inhibition by BAY-299 shows efficacy *in vivo*

To assess BRD1 inhibitor efficacy *in vivo*, BAY-299 was tested in a syngeneic PAX8-positive ovarian cancer mouse model generated with STOSE cells (21). A MTD study was performed in female FVB/N mice. The drug was well tolerated with no side effects at the maximum dose.

For the *in vivo* experiment (**Fig. 7G**, top), 20 FVB/N female mice were injected with STOSE cells on day 1, and 18 days later, daily vehicle or BAY-299 treatments were initiated. Eighteen days after treatment initiation the mice were weighed, euthanized, and the tumor burden and immune composition analyzed (**Fig. 7G**).

Final animal weights were similar in both treatment groups (Supplementary Fig. S15A). Grossly visible solid tumor was dissected from all animals and appeared histologically similar in both groups forming sheets and clusters of neoplastic epithelioid cells with cytomorphologic features consistent with a poorly differentiated Müllerian carcinoma (Supplementary Fig. S15B). Tumor volumes were given a score of 0–3 (3 being highest), and most of the vehicle-treated mice scored highest while the majority of the BAY-299 scored lowest (**Fig. 7H**). Most of the vehicle-treated animals had high volume ascites correlating with high solid tumor burden, while most of the BAY-299–treated animals had little to no ascites correlating with low tumor burden (**Fig. 7I**).

We characterized solid tumors, ascites, and spleens for immune composition (T- and NK-cell quantity), exhaustion marker expression (TIM3, PD-1, and PD-L1), and activation marker expression (IFNγ, GZMB, Ki67; **Fig. 7J**; and **K**; Supplementary Fig. S15C–S15I). Given the low tumor burden and ascites volume in BAY-299–treated animals, samples were combined from multiple animals for analysis for each individual tissue/treatment type. Flow cytometry analysis of the spleens did not demonstrate shifts in T- or NK-cell populations (Supplementary Fig. S15C and S15E).

Flow cytometry analysis of the solid tumors demonstrated an increase in NK cells and CD8 T cells after BAY-299 treatment (**Fig. 7J**). NK-cell antibodies for markers NK-1.1 and NKp46 were utilized (48) with limited overlap in the CD3⁻/NK-1.1⁺ and CD3⁻/NKp46⁺ groups. The NKp46⁺ NK cells expanded after BAY-299 treatment in the solid tumors (**Fig. 7J**; Supplementary Fig. S15F). Assessment of exhaustion markers post-treatment demonstrated a decrease in PD-1 expression on CD8 T and both NK-1.1 and NKp46⁺ NK cells (**Fig. 7K**) similar to bispecific antibody (**Fig. 5**) and BAY-299 treatments (**Fig. 6**) in organoid co-cultures. TIM3 and PD-1/TIM3 coexpression and activation and killing marker expression was similar between treatments.

Conversely, in the ascites, only two BAY-299–treated samples showed CD8 T-cell expansion and NK-1.1⁺ NK cells expanded post-treatment (Supplementary Fig. S15D and S15G). TIM3 expression decreased post-treatment on both NK-1.1 and NKp46⁺ NK cells (Supplementary Fig. S15H) similar to the bispecific antibody (**Fig. 5**) and BAY-299 treatments (**Fig. 6**) in organoid co-cultures. TIM3 and PD-1/TIM3 coexpression was similar between treatments. Activation and killing markers were assessed, and CD107A mildly increased in both the NK-1.1 and NKp46⁺ NK cells post-treatment (Supplementary Fig. S15I).

Altogether, these results suggest that *BRD1* depletion is likely an underlying mechanism for the superiority of the bispecific antibody and that, like the bispecific antibody, BRD1 inhibition leads to

decreased immune exhaustion and increased immune activation, particularly in NK cells, which may make it an effective immune target in HGSC.

Discussion

The major cellular and mechanistic targets of ICB therapies in HGSC have not been defined making designing more effective therapies and identifying patients who might benefit from immune therapy difficult. Using real-time functional analysis of novel HGSC organoid-immune cell co-cultures treated with a novel bispecific antibody and its monospecific controls, we identified three critical cellular and mechanistic immune therapy targets in HGSC. This led to the identification of two novel immune therapies that may have increased activity in patients with HGSC, a bispecific anti-PD-1/PD-L1 antibody and BRD1 inhibitor, both of which show in vivo anti-tumor efficacy, suggesting further therapeutic exploration of these agents may be merited (**Fig. 7** and ref. 19).

Key to understanding the molecular functions of ICB agents in HGSC was our ability to gain a comprehensive appreciation of the effects of these agents on every cell in the tumor in novel HGSC organoid co-cultures (**Figs. 2–6**). Our most striking findings were in NK and T cells. Mechanisms of tumor microenvironment–induced NK-cell dysfunction and NK response to ICB agents are undefined (8, 16). We found that the bispecific antibody and the BRD1 inhibitor BAY-299 induced strong NK-cell activation through induction of a state change from an inert and exhausted to a more active and cytotoxic phenotype, which correlated with in vivo efficacy of these agents (**Figs. 2**, **4–7**; ref. 19). In so doing, we define NK-cell activation as a key component of therapeutic efficacy for immune therapy agents in HGSC that is lacking with currently used ICB agents.

In addition, our analysis demonstrated which CD8 T cells are most critical for ICB response in HGSC. We find that all three ICB agents, particularly the bispecific antibody, induced a transition from (i) naïve to cytotoxic progenitor-exhausted groups, and (ii) terminally exhausted to progenitor-exhausted cytotoxic groups (**Fig. 5**). This suggests that the ICB-driven naïve to cytotoxic progenitor transition may drive response in the long term and suggest that identifying therapies that can induce this state change may be important.

We determined that these state changes were being driven, in part, by bispecific antibody downregulation of *BRD1* expression (**Fig. 6**). Bromodomain proteins such as BRD1 and BRD4 play roles in immune and hematologic cell development and modulation of tumor inflammation (36, 37, 49) but are often targeted with the goal of affecting changes within the tumor cells as a means of therapeutic efficacy (38, 49, 50). Our findings led us to explore the novel role of BRD1 and BRD1 inhibitors in the immune cells instead.

Here we show BRD1 inhibition induces NK and some CD8 T cells into more active states by reducing exhaustion, and that this can enhance the activity of ICB agents like pembrolizumab in vitro (**Fig. 6**). The mechanism of action of BRD1 inhibition in these changes likely involves key epigenetic alterations (**Fig. 7A–C**); however, further work will be needed to fully understand this complex process. In addition, BAY-299 demonstrated increased efficacy in decreasing tumor burden in vivo through decreasing exhaustion of NK and CD8 T cells (**Fig. 7**). Overall, these findings suggest that BRD1 inhibition may be effective at enhancing the anti-tumor immune response and merit further exploration as a therapeutic option either alone or in relevant combinations in HGSC. In addition, this discovery in organoid co-cultures high-lights the importance of studying the effects of any agent, even those thought to target intrinsic tumor cell properties, on every cell in a tumor. This may lead to unexpected discoveries that open up a broader array of small-molecule therapies in the immune space due to unanticipated effects of therapeutic agents on the immune compartment.

Overall, this work suggests the potential for HGSCs to be effectively targeted with immune therapies if the therapies engage the correct mechanistic pathways in the right immune cell types. These findings highlight a common immune therapy problem across HGSCs. It is not a tumor cell genomic or molecular defect making only some HGSCs responsive to these agents, rather it is a state of dysfunction in different subsets of CD8 T cells and NK cells driven by the solid tumor microenvironment blocking current ICB response across HGSCs. By gaining a better understanding of the mechanisms driving these dysfunctional states and how to overcome them, as we have begun to do here using a novel model system and novel therapeutic tool, we have identified available therapies to offer patients with HGSC, like BRD1 inhibitors, which effectively target these pathways. Mechanism-driven therapies have the potential to someday make immune therapy effective in HGSC, a deadly disease where it has not been effective before.

Authors' Contributions

C. Wan: Formal analysis, methodology, writing-original draft, writing-review and editing. M.P. Keany: Data curation, writing-original draft, writing-review and editing. H. Dong: Data curation, writing-original draft. L.F. Al-Alem: Resources, data curation, formal analysis, investigation, writing-review and editing. U.M. Pandya: Resources, data curation, formal analysis, investigation, writing-review and editing. S. Lazo: Data curation, writing-original draft, writing-review and editing. K. Boehnke: Data curation, writing-review and editing. K.N. Lynch: Data curation, investigation, writing-review and editing. R. Xu: Investigation, writing-review and editing. D.T. Zarrella: Investigation, writing-review and editing. S. Gu: Data curation, writing-original draft, writing-review and editing. P. Cejas: Resources, writing-review and editing. K. Lim: Resources, writing-review and editing. H.W. Long: Resources, writing-review and editing. K.M. Elias: Resources, writing-original draft, writing-review and editing. N.S. Horowitz: Resources, writing-original draft, writing-review and editing. C.M. Feltmate: Resources, writing-original draft, writing-review and editing. M.G. Muto: Resources, writing-original draft, writing-review and editing. M.J. Worley: Resources, writing-original draft, writing-review and editing. R.S. Berkowitz: Resources, writing-original draft, writing-review and editing. U.A. Matulonis: Resources, writing-review and editing. M.R. Nucci: Resources, writing-review and editing. C.P. Crum: Resources, writing-review and editing. B.R. Rueda: Resources, formal analysis, funding acquisition, investigation, writing-review and editing. M. Brown: Data curation, writing-review and editing. X.S. Liu: Data curation, writing-review and editing. S.J. Hill: Conceptualization, resources, data curation, formal analysis, supervision, funding acquisition, validation, investigation, visualization, methodology, writing-original draft, project administration, writing-review and editing.

Wan et al.

References

1. Siegel RL, Miller KD, Jemal A. Cancer statistics, 2019. CA Cancer J Clin 2019;69: 7–34.
2. Narod S. Can advanced-stage ovarian cancer be cured? Nat Rev Clin Oncol 2016; 13:255–61.
3. Ghisoni E, Imbimbo M, Zimmermann S, Valabrega G. Ovarian cancer immunotherapy: turning up the heat. Int J Mol Sci 2019;20:2927.
4. Odunsi K. Immunotherapy in ovarian cancer. Ann Oncol 2017;28:viii1–viii7.
5. Thorsson V, Gibbs DL, Brown SD, Wolf D, Bortone DS, Ou Yang TH, et al. The immune landscape of cancer. Immunity 2018;48:812–30.e14.
6. Sato E, Olson SH, Ahn J, Bundy B, Nishikawa H, Qian F, et al. Intraepithelial CD8+ tumor-infiltrating lymphocytes and a high CD8+/regulatory T cell ratio are associated with favorable prognosis in ovarian cancer. Proc Natl Acad Sci U S A 2005;102:18538–43.
7. Zhang L, Conejo-Garcia JR, Katsaros D, Gimotty PA, Massobrio M, Regnani G, et al. Intratumoral T cells, recurrence, and survival in epithelial ovarian cancer. N Engl J Med 2003;348:203–13.
8. Hoogstad-van Evert JS, Bekkers R, Ottevanger N, Jansen JH, Massuger L, Dolstra H. Harnessing natural killer cells for the treatment of ovarian cancer. Gynecol Oncol 2020;157:810–6.
9. Hoogstad-van Evert JS, Maas RJ, van der Meer J, Cany J, van der Steen S, Jansen JH, et al. Peritoneal NK cells are responsive to IL-15 and percentages are correlated with outcome in advanced ovarian cancer patients. Oncotarget 2018;9:34810–20.
10. Miller BC, Sen DR, Al Abosy R, Bi K, Virkud YV, LaFleur MW, et al. Subsets of exhausted CD8(+) T cells differentially mediate tumor control and respond to checkpoint blockade. Nat Immunol 2019;20:326–36.
11. Yost KE, Satpathy AT, Wells DK, Qi Y, Wang C, Kageyama R, et al. Clonal replacement of tumor-specific T cells following PD-1 blockade. Nat Med 2019; 25:1251–9.
12. Wherry EJ, Kurachi M. Molecular and cellular insights into T cell exhaustion. Nat Rev Immunol 2015;15:486–99.
13. da Silva IP, Gallois A, Jimenez-Baranda S, Khan S, Anderson AC, Kuchroo VK, et al. Reversal of NK-cell exhaustion in advanced melanoma by Tim-3 blockade. Cancer Immunol Res 2014;2:410–22.
14. Thommen DS, Schumacher TN. T cell dysfunction in cancer. Cancer Cell 2018; 33:547–62.
15. Philip M, Fairchild L, Sun L, Horste EL, Camara S, Shakiba M, et al. Chromatin states define tumour-specific T cell dysfunction and reprogramming. Nature 2017;545:452–6.
16. Sun H, Sun C. The rise of NK cell checkpoints as promising therapeutic targets in cancer immunotherapy. Front Immunol 2019;10:2354.
17. Jenkins RW, Aref AR, Lizotte PH, Ivanova E, Stinson S, Zhou CW, et al. *Ex vivo* profiling of PD-1 blockade using organotypic tumor spheroids. Cancer Discov 2018;8:196–215.
18. Neal JT, Li X, Zhu J, Giangarra V, Grzeskowiak CL, Ju J, et al. Organoid modeling of the tumor immune microenvironment. Cell 2018;175:1972—88.e16.
19. Kotanides H, Li Y, Malabunga M, Carpenito C, Eastman SW, Shen Y, et al. Bispecific targeting of PD-1 and PD-L1 enhances T-cell activation and antitumor immunity. Cancer Immunol Res 2020;8:1300–10.
20. Stoeckius M, Zheng S, Houck-Loomis B, Hao S, Yeung BZ, Mauck WM 3rd, et al. Cell Hashing with barcoded antibodies enables multiplexing and doublet detection for single cell genomics. Genome Biol 2018;19:224.
21. McCloskey CW, Goldberg RL, Carter LE, Gamwell LF, Al-Hujaily EM, Collins O, et al. A new spontaneously transformed syngeneic model of high-grade serous ovarian cancer with a tumor-initiating cell population. Front Oncol 2014;4:53.
22. Gitto SB, Kim H, Rafail S, Omran DK, Medvedev S, Kinose Y, et al. An autologous humanized patient-derived-xenograft platform to evaluate immunotherapy in ovarian cancer. Gynecol Oncol 2020;156:222–32.
23. Friese C, Harbst K, Borch TH, Westergaard MCW, Pedersen M, Kverneland A, et al. CTLA-4 blockade boosts the expansion of tumor-reactive CD8(+) tumor-infiltrating lymphocytes in ovarian cancer. Sci Rep 2020;10:3914.
24. Balkwill FR, Mantovani A. Cancer-related inflammation: common themes and therapeutic opportunities. Semin Cancer Biol 2012;22:33–40.
25. Li Y, Carpenito C, Wang G, Surguladze D, Forest A, Malabunga M, et al. Discovery and preclinical characterization of the antagonist anti-PD-L1 monoclonal antibody LY3300054. J Immunother Cancer 2018;6:31.
26. Zamarin D, Burger RA, Sill MW, Powell DJ Jr, Lankes HA, Feldman MD, et al. Randomized phase II trial of nivolumab versus nivolumab and ipilimumab for recurrent or persistent ovarian cancer: an NRG oncology study. J Clin Oncol 2020;38:1814–23.
27. Labrijn AF, Janmaat ML, Reichert JM, Parren P. Bispecific antibodies: a mechanistic review of the pipeline. Nat Rev Drug Discov 2019;18:585–608.
28. Ayers M, Lunceford J, Nebozhyn M, Murphy E, Loboda A, Kaufman DR, et al. IFN-gamma-related mRNA profile predicts clinical response to PD-1 blockade. J Clin Invest 2017;127:2930–40.
29. Stuart T, Butler A, Hoffman P, Hafemeister C, Papalexi E, Mauck WM 3rd, et al. Comprehensive integration of single-cell data. Cell 2019;177:1888–902.e21.
30. Romee R, Rosario M, Berrien-Elliott MM, Wagner JA, Jewell BA, Schappe T, et al. Cytokine-induced memory-like natural killer cells exhibit enhanced responses against myeloid leukemia. Sci Transl Med 2016;8:357ra123.
31. Del Zotto G, Marcenaro E, Vacca P, Sivori S, Pende D, Della Chiesa M, et al. Markers and function of human NK cells in normal and pathological conditions. Cytometry B Clin Cytom 2017;92:100–14.
32. Dong H, Adams NM, Xu Y, Cao J, Allan DSJ, Carlyle JR, et al. The IRE1 endoplasmic reticulum stress sensor activates natural killer cell immunity in part by regulating c-Myc. Nat Immunol 2019;20:865–78.
33. Morvan MG, Lanier LL. NK cells and cancer: you can teach innate cells new tricks. Nat Rev Cancer 2016;16:7–19.
34. Loftus RM, Assmann N, Kedia-Mehta N, O'Brien KL, Garcia A, Gillespie C, et al. Amino acid-dependent cMyc expression is essential for NK cell metabolic and functional responses in mice. Nat Commun 2018;9:2341.
35. Haghverdi L, Buettner F, Theis FJ. Diffusion maps for high-dimensional single-cell analysis of differentiation data. Bioinformatics 2015;31:2989–98.
36. Mishima Y, Miyagi S, Saraya A, Negishi M, Endoh M, Endo TA, et al. The Hbo1-Brd1/Brpf2 complex is responsible for global acetylation of H3K14 and required for fetal liver erythropoiesis. Blood 2011;118:2443–53.
37. Mishima Y, Wang C, Miyagi S, Saraya A, Hosokawa H, Mochizuki-Kashio M, et al. Histone acetylation mediated by Brd1 is crucial for Cd8 gene activation during early thymocyte development. Nat Commun 2014;5:5872.
38. Bouche L, Christ CD, Siegel S, Fernandez-Montalvan AE, Holton SJ, Fedorov O, et al. Benzoisoquinolinediones as potent and selective inhibitors of BRPF2 and TAF1/TAF1L bromodomains. J Med Chem 2017;60:4002–22.
39. Li B, Severson E, Pignon JC, Zhao H, Li T, Novak J, et al. Comprehensive analyses of tumor immunity: implications for cancer immunotherapy. Genome Biol 2016; 17:174.
40. Jin HT, Anderson AC, Tan WG, West EE, Ha SJ, Araki K, et al. Cooperation of Tim-3 and PD-1 in CD8 T-cell exhaustion during chronic viral infection. Proc Natl Acad Sci U S A 2010;107:14733–8.
41. Yagita M, Huang CL, Umehara H, Matsuo Y, Tabata R, Miyake M, et al. A novel natural killer cell line (KHYG-1) from a patient with aggressive natural killer cell leukemia carrying a p53 point mutation. Leukemia 2000;14:922–30.

42. Hafner M, Niepel M, Chung M, Sorger PK. Growth rate inhibition metrics correct for confounders in measuring sensitivity to cancer drugs. Nat Methods 2016;13:521–7.

43. Wang D, Malarkannan S. Transcriptional regulation of natural killer cell development and functions. Cancers 2020;12:1591.

44. Hertweck A, Evans CM, Eskandarpour M, Lau JC, Oleinika K, Jackson I, et al. T-bet activates Th1 genes through mediator and the super elongation complex. Cell Rep 2016;15:2756–70.

45. Zhang H, Pandey S, Travers M, Sun H, Morton G, Madzo J, et al. Targeting CDK9 reactivates epigenetically silenced genes in cancer. Cell 2018;175:1244–58.e26.

46. Yang C, Siebert JR, Burns R, Zheng Y, Mei A, Bonacci B, et al. Single-cell transcriptome reveals the novel role of T-bet in suppressing the immature NK gene signature. Elife 2020;9:e51339.

47. Hill SJ, Decker B, Roberts EA, Horowitz NS, Muto MG, Worley MJ Jr, et al. Prediction of DNA repair inhibitor response in short-term patient-derived ovarian cancer organoids. Cancer Discov 2018; 8:1404–21.

48. Walzer T, Blery M, Chaix J, Fuseri N, Chasson L, Robbins SH, et al. Identification, activation, and selective *in vivo* ablation of mouse NK cells via NKp46. Proc Natl Acad Sci U S A 2007;104:3384–9.

49. White ME, Fenger JM, Carson WE 3rd. Emerging roles of and therapeutic strategies targeting BRD4 in cancer. Cell Immunol 2019; 337:48–53.

50. Sun C, Yin J, Fang Y, Chen J, Jeong KJ, Chen X, et al. BRD4 inhibition is synthetic lethal with PARP inhibitors through the induction of homologous recombination deficiency. Cancer Cell 2018;33:401–16.e8.

Cancer Research

AAC R American Association for Cancer Research

Enhanced Efficacy of Simultaneous PD-1 and PD-L1 Immune Checkpoint Blockade in High-Grade Serous Ovarian Cancer

Changxin Wan, Matthew P. Keany, Han Dong, et al.

Updated version	Access the most recent version of this article at: doi:10.1158/0008-5472.CAN-20-1674
Supplementary Material	Access the most recent supplemental material at: http://cancerres.aacrjournals.org/content/suppl/2020/11/06/0008-5472.CAN-20-1674.DC1

Cited articles	This article cites 50 articles, 10 of which you can access for free at: http://cancerres.aacrjournals.org/content/81/1/158.full#ref-list-1

E-mail alerts	Sign up to receive free email-alerts related to this article or journal.
Reprints and Subscriptions	To order reprints of this article or to subscribe to the journal, contact the AACR Publications Department at pubs@aacr.org.
Permissions	To request permission to re-use all or part of this article, use this link http://cancerres.aacrjournals.org/content/81/1/158. Click on "Request Permissions" which will take you to the Copyright Clearance Center's (CCC) Rightslink site.